bioRxiv preprint doi: https://doi.org/10.1101/2023.02.20.529089; this version posted February 21, 2023. The copyright holder for this preprint (which was not certified by peer review) is the author/funder. All rights reserved. No reuse allowed without permission.

Mechanisms of neutralizing antibody response probed using synthetic virus-like structures

Wei-Yun Wholey[1†], Alexander R. Meyer[1†], Sekou-Tidiane Yoda[1], Bryce Chackerian[2], Julie Zikherman[3], Wei Cheng[1,4]*

[1]*Department of Pharmaceutical Sciences, 428 Church Street, University of Michigan, Ann Arbor, Michigan 48109, USA*

[2]*Department of Molecular Genetics and Microbiology, School of Medicine, University of New Mexico, Albuquerque, New Mexico 87131, USA*

[3]*Division of Rheumatology, Rosalind Russell and Ephraim P. Engleman Arthritis Research Center, Department of Medicine, University of California, San Francisco, California 94143 USA*

[4]*Department of Biological Chemistry, 1150 W. Medical Center Dr., University of Michigan Medical School, Ann Arbor, Michigan 48109, USA*

*Corresponding author:

Dr Wei Cheng
University of Michigan
428 Church Street
Ann Arbor, MI, 48109-1065
Tel: (734) 763-3709
Fax: (734) 615-6162

email address: chengwe@umich.edu

Keywords: antibody, virus-like structures, epitope density, nucleic acids

†: Both authors contributed equally to this work.

bioRxiv preprint doi: https://doi.org/10.1101/2023.02.20.529089; this version posted February 21, 2023. The copyright holder for this preprint (which was not certified by peer review) is the author/funder. All rights reserved. No reuse allowed without permission.

ABSTRACT

Class-switched neutralizing antibody production is rapidly induced upon many viral infections and often long-lived, but the underlying mechanisms remain incompletely understood. Here we show that several features of this antibody response can be reconstituted by synthetic virus-like structures containing minimal, highly purified biochemical ingredients commonly found in enveloped viruses, and without viral replication or any other adjuvants. These findings reveal a shared mechanism for the production of neutralizing antibodies upon viral infection. High epitope density is capable but not necessary for driving antibody secretion. Instead, even a few molecules of surface antigen, when combined with nucleic acids within these structures, can trigger strong antiviral IgG production. As a result, B cells integrate both signals from individual viral particulate antigens to initiate a neutralizing IgG response.

One-sentence summary

Reconstitution of minimal viral signals necessary to trigger antiviral IgG

bioRxiv preprint doi: https://doi.org/10.1101/2023.02.20.529089; this version posted February 21, 2023. The copyright holder for this preprint (which was not certified by peer review) is the author/funder. All rights reserved. No reuse allowed without permission.

Studies of humoral immunity upon viral infection have revealed many common features of antibody responses towards both icosahedral and enveloped viruses (*1-5*). For the majority of viruses, these antibodies are induced rapidly, within just a few days after infection (*4*). These early antibodies are isotype class-switched independent of $CD4^+$ T cells (*6-10*), and are potent in viral neutralization (*6, 8-10*). In some cases, the antibody production can last very long after the resolution of primary infections (*5, 11, 12*). These common features suggest shared mechanisms in B cell sensing and response to viral particulate antigens (Ags). However, the mechanisms responsible for these neutralizing antibody (nAb) responses remain incompletely understood. The minimal biochemical and biophysical signals from viruses that are necessary to initiate a nAb response *in vivo* remain debated (*3, 13*).

To understand the mechanisms of B cell responses to viral particulate Ags, we have developed a reductionist system of synthetic virus-like structures (SVLS) that are constructed using highly purified biochemical ingredients and resemble the common biophysical features of naturally occurring enveloped viruses (*14-16*). Existing platforms such as virus-like particles (VLPs) (*17, 18*), ferritin nanoparticles (*19*) or computationally designed self-assembling protein nanomaterials (*20*) have been extensively studied and used in vaccine design and development (*21-23*). However, they all use immunogenic foreign proteins as their structural scaffolds for antigen display. To unravel the molecular basis of virion immunogenicity, the SVLS system herein uses lipid bilayers (*24-26*) instead of foreign proteins to serve as the scaffold of SVLS, eliminating immune responses towards the scaffolds themselves, which may complicate data interpretation. In fact, we selectively chose lipids that were abundant in natural plasma membranes to construct SVLS (Materials and Methods). To mimic naturally occurring viruses, we also avoided cationic lipids that are known to be immunostimulatory in nature (*27*), which were extensively used especially

bioRxiv preprint doi: https://doi.org/10.1101/2023.02.20.529089; this version posted February 21, 2023. The copyright holder for this preprint (which was not certified by peer review) is the author/funder. All rights reserved. No reuse allowed without permission.

recently for the therapeutic delivery of nucleic acids (*28*). In addition, this system allows us to encapsulate internal nucleic acids (iNA) with *all-natural* phosphodiester backbone inside SVLS, which mimics the spatial confinement and chemical composition of a typical viral genome (*15, 16*). The role of encapsulated nucleic acids on long-term nAb responses has not been investigated using either ferritin or computationally designed self-assembling protein nanomaterials.

We have prepared four sets of SVLS for current study: two of them, schematically shown in Fig. 1A and B insets and termed pRBD and pHEL, respectively, are SVLS that display either purified receptor-binding domain (RBD) of the SARS-CoV-2, the causative agent of the COVID-19 pandemic (*29*); or a purified hen egg lysozyme (HEL) mutant, a well-established model antigen for immunology studies. Each protein was displayed in specific orientation at regulated densities on the surface of SVLS. The interior of pRBD and pHEL was filled with phosphate buffered saline (PBS). The other two sets: pRBD(iNA) and pHEL(iNA), schematically shown in Fig. 1C and D insets, are SVLS that not only display RBD or HEL on their surface, but also encapsulate nucleic acids inside these structures. All protein display was achieved through site-specific covalent conjugation on the lipid bilayer surface to ensure stability of the attachment with time (*14-16*). No proteins other than RBD or HEL were present in these structures. Fig. 1A through D show dynamic light scattering measurements of these structures, with diameters around 120 nm, which is very close to that of HIV, influenza virus and SARS-CoV-2 (*30-32*). Fig. 1E show a representative epi-fluorescence image of individual pRBD(iNA) stained by a fluorescent RBD-specific Fab (Fig. S1). We determined the average number of antigenic molecules per structure, termed epitope density (ED) herein, using both ensemble and single-molecule fluorescence techniques that we established previously (*33-35*). As shown in Table S1, we produced SVLS with a range of

bioRxiv preprint doi: https://doi.org/10.1101/2023.02.20.529089; this version posted February 21, 2023. The copyright holder for this preprint (which was not certified by peer review) is the author/funder. All rights reserved. No reuse allowed without permission.

EDs for these structures that well covers the EDs observed for naturally occurring viruses (*36, 37*). As shown in Fig. 1F, the values of ED for pRBD(iNA) that we measured using a single-molecule fluorescence method (Fig. S1) overall agreed with ED values from ensemble-based measurement, even at low EDs. This is very important especially when we intend to assess the impact of just a few molecules of Ag per SVLS on B cell antibody production.

Most viruses infect their hosts through peripheral routes (*38*). To simulate a natural viral infection using SVLS, we delivered a submicrogram dose of Ag into mice through subcutaneous injection of SVLS. Subcutaneous injection allows viral collection by the initial lymphatics to encounter B cells in the lymph nodes (*39*). A submicrogram dose of Ag is equivalent to picomoles of SVLS, which is a very low dose of Ag compared to those typically used in vaccines comprised of VLPs (*18, 40-42*) and computationally designed self-assembling protein nanomaterials (*22, 23*); and comparable to the Ag dose used in ferritin nanoparticle immunization (*21*). Natural viral infection does not involve any conventional adjuvants such as alum. To mimic this aspect, throughout, all the injections were performed in the absence of any exogenous adjuvants. As a result, the injections only introduced the highly purified protein Ags and lipids for pRBD or pHEL, and the Ags, lipids and purified nucleic acids for pRBD(iNA) or pHEL(iNA). Moreover, all the SVLS were sterile filtered through 0.45 µm membranes before injections.

To our surprise, we found that a single injection of pRBD or pHEL at submicrogram Ag dose and in the absence of iNA or any other adjuvants is sufficient to elicit a fast onset of Ag-specific IgG response in both C57BL/6 (B6) and BALB/c mice, provided that the ED on SVLS was above an apparent threshold (*43*). This is shown in Fig. 2A and 2B for various

bioRxiv preprint doi: https://doi.org/10.1101/2023.02.20.529089; this version posted February 21, 2023. The copyright holder for this preprint (which was not certified by peer review) is the author/funder. All rights reserved. No reuse allowed without permission.

conditions that we tested using pRBD and pHEL, respectively. For both SVLS, the Ag-specific IgG could be detected as early as day 5 post injection (D5, circles), with stronger responses on Day 11 (D11, columns) (Fig. 2A-2B, Conditions 6 and 7). The Ag-specific IgG responses were absent in several controls including PBS (Condition 1), soluble proteins (sRBD or sHEL, Condition 2), or an admixture of soluble proteins and control SVLS without conjugated proteins on the surface or iNA (Condition 3). In fact, a dose escalation of either sRBD or sHEL by tenfold could not elicit any detectable Ag-specific IgG through the same procedure. The exquisite sensitivity of animals towards pRBD or pHEL suggests that there are distinct signalling mechanisms involved in the sensing of these particulate Ags (*44*). In fact, in vitro studies using the same system of pHEL revealed that these SVLS were over 1000-fold more potent than respective soluble proteins in activation of Ag-specific B cells (*44*). Fig. 2A and Fig. 2B also revealed apparent thresholds of ED for IgG induction by either pRBD or pHEL in B6 mice. At the same Ag dose, an ED less than 20 was not sufficient to induce an Ag-specific IgG above background for either pRBD or pHEL (Fig. 2A-2B, Conditions 4 and 5). The IgG response increased with increasing ED for both pRBD and pHEL above the respective thresholds. Importantly, the animal sera from pRBD immunization as in Conditions 6 and 7 could effectively neutralize HIV-1 pseudovirions (*45*) that displayed the cognate S protein of the SARS-CoV-2 *in vitro* (Fig. 2C), suggesting that the antibodies present in these sera would be functional *in vivo* to offer host protection against infection of SARS-CoV-2. For both pRBD and pHEL, this fast IgG response induced IgG1, IgG2b and IgG3 in B6 mice (Fig. 2D-I), with very low or undetectable IgM or IgG2c (Fig. S2), which shows similarity to the subclasses of IgG induced in the context of live viral infections (*8*) yet distinct from those induced by the type II T-independent Ags (*46*). These results suggest distinct actions of these SVLS in triggering class-switch recombination of the Ag-specific B cells *in vivo*. The presence of the HEL-specific IgG in B6 mice is surprising

bioRxiv preprint doi: https://doi.org/10.1101/2023.02.20.529089; this version posted February 21, 2023. The copyright holder for this preprint (which was not certified by peer review) is the author/funder. All rights reserved. No reuse allowed without permission.

because it is well established that the B6 strain is unresponsive to HEL due to its failure to generate a dominant MHC Class II determinant (*47*), which suggests that the initiation of the fast nAb response by these SVLS is independent of T cells. To test this, we immunized B6 mice that were deficient in both alpha beta and gamma delta T-cell receptors ($TCR^{-/-}$) (*48*) with either pRBD or pHEL. Statistical comparisons between Condition 7 (wild-type B6 or wtB6) and Condition 8 ($TCR^{-/-}$) for pRBD4 in Fig. 2A or between Condition 6 (wtB6) and Condition 8 ($TCR^{-/-}$) for pHEL3 in Fig. 2B for both D5 and D11 did not reveal significant differences (p-values>0.1 for all cases), suggesting that this IgG response was largely T-independent for both Ags. Furthermore, the nAb response was also observed in B6 mice that were deficient in MyD88 (*49*) ($MyD88^{-/-}$) (Condition 9 in Fig. 2). Comparisons with respective wtB6 mice for both D5 and D11 did not reveal significant differences between Condition 7 (wtB6) and Condition 9 ($MyD88^{-/-}$) for pRBD4 in Fig. 2A or between Condition 6 (wtB6) and Condition 9 ($MyD88^{-/-}$) for pHEL3 in Fig. 2B (p-values>0.1 for all cases). These data ruled out the possibility that endotoxin or nucleic acid contamination of the SVLS produced these T-independent nAb responses, and suggest that the oriented display of foreign Ags above a threshold ED on a virion-sized liposome can provide a sufficient '*external*' signal to trigger a fast nAb response. And this antibody response is in the absence of Toll-like receptor signalling (*50*). Consistent with these results, our studies using the same system of pHEL on Ag-specific B cells *in vitro* revealed that pHEL alone, without any exogenous adjuvants, can trigger robust B cell proliferation and survival in the absence of MyD88, IRAK1/4 and CD40 ligation (*44*). Moreover, the nAb response induced by pRBD or pHEL was completely abrogated in B6 mice that were deficient in CD19 ($CD19^{-/-}$) (*51*) (Condition 10). CD19 is an important coreceptor on B cells (*52*). It lowers the threshold for B cell antigen receptor activation (*53*) and is essential for B cell responses to membrane-bound

bioRxiv preprint doi: https://doi.org/10.1101/2023.02.20.529089; this version posted February 21, 2023. The copyright holder for this preprint (which was not certified by peer review) is the author/funder. All rights reserved. No reuse allowed without permission.

ligands (*54*). These data indicate that CD19 is required for B cell production of IgG in response to these SVLS in the absence of iNA *in vivo*.

Compared to wtB6 mice, BALB/c mice also mounted a similar nAb response on D5 after immunization with pRBD or pHEL (Fig. 2J circles): the sera from pRBD injected mice could neutralize pseudovirions *in vitro* (*16*). The IgG response induced IgG1, IgG2b and IgG3, with low or undetectable Ag-specific IgM or IgG2a (Fig. S3). The presence of these similarities with B6 suggests that the early nAb response is an immediate host response that is conserved in both strains of mice. However, the IgG response in BALB/c mice on D11 was much higher than those in wtB6 mice (Fig. 2J columns), due to a much stronger IgG1 response that dominated on D11 for both pRBD and pHEL (Fig. S3B and S3G), suggesting that there are major differences between the two mouse strains in the amplification of the nAb response beyond D5 after its initial activation.

To gain more insight into the differences between the two strains of mice in their responses to SVLS, we collected inguinal lymph nodes from both animals on D12 after a single injection of pRBD and stained cells for identification by flow cytometry. As shown in Fig. S4A and Fig. S4D for $CD19^+$ gated live lymphocytes in wtB6 and BALB/c mice respectively, we could clearly identify $GL7^+$ cells induced by pRBD well above those from either PBS (Condition 1) or soluble protein (Condition 2) immunized controls (Fig. S4B, S4E) for both wtB6 and BALB/c mice. However, we noticed that BALB/c mice consistently had higher percentages of Ag-induced $GL7^+$ B cells than those in wtB6. Comparison between wtB6 and BALB/c mice using one-way ANOVA test for Condition 3 returned a p-value of 6.4×10^{-7} and a p-value of 2.3×10^{-4} for Condition 4 between wtB6 and BALB/c mice, indicating statistical significance of these differences. Within these $CD19^+GL7^+$ cells, we identified $CD38^-CD95^+$

bioRxiv preprint doi: https://doi.org/10.1101/2023.02.20.529089; this version posted February 21, 2023. The copyright holder for this preprint (which was not certified by peer review) is the author/funder. All rights reserved. No reuse allowed without permission.

populations that corresponded to germinal center (GC) B cells in both wtB6 and BALB/c mice (Q1 in Fig. S4C, S4F). Consistent with lower percentages of $GL7^+$ B cells, the number of GC B cells induced by pRBD was much lower in wtB6 than BALB/c mice (p-value = 7.7×10^{-5} from one-way ANOVA test, N=4) under the same set of conditions. These data confirmed that B cell responses were initiated in both strains of animals upon a single exposure to submicrogram dose of pRBD, but the responses beyond D5 were amplified very differently.

Neither pRBD nor pHEL have iNA in their interiors. To examine the impact of iNA with natural phosphodiester backbones on the above nAb response, we administered a single subcutaneous injection of pRBD(iNA) or pHEL(iNA) to mice at submicrogram Ag dose without the use of additional adjuvants. As shown in Fig. 3A and 3C for various conditions that we have tested for pRBD(iNA) and pHEL(iNA), we first measured the Ag-specific IgG responses in mice of B6 genetic backgrounds on both D5 (circles) and D11 (columns) post injection using ELISA. These conditions included controls, SVLS of different ED, different iNA sequences in either wtB6 or various gene knockout mice, as illustrated on the right in Fig. 3A and 3C. Many of these conditions induced strong Ag-specific IgG as early as D5 post injection, resulting in ELISA OD450 values >2. For correct interpretation of the data, we thus determined IgG titers for most conditions, as shown in Fig. 3B and 3D for pRBD(iNA) and pHEL(iNA), respectively. First, we observed a strong synergy between ED and iNA for SVLS encapsulating DNA1, a 20-mer single-stranded DNA that harbors two unmethylated CpG dinucleotides but has an all-natural phosphodiester backbone (Materials and Methods), as shown by Conditions 4 through 7 for both RBD and HEL. When compared to either pRBD or pHEL without iNA, the titers of the IgG induced by these SVLS with DNA1 in wtB6 were all 10- to 1000-fold higher on D5 (circles, Fig. 3B and 3D), with an

bioRxiv preprint doi: https://doi.org/10.1101/2023.02.20.529089; this version posted February 21, 2023. The copyright holder for this preprint (which was not certified by peer review) is the author/funder. All rights reserved. No reuse allowed without permission.

even stronger response on D11 (columns). As demonstrated by several controls in Fig. 3A and C, the simultaneous presence of ED and iNA on the same SVLS was necessary for the strong and rapid responses observed. Condition 1 is an admixture of soluble proteins with DNA1. Condition 2 and 3 are admixtures of DNA1 and SVLS of different ED without iNA. Although unmethylated CpG DNA can activate Toll-like receptor 9 (TLR9) (*55*), neither Condition 1 nor Condition 2 elicited Ag-specific IgG. Condition 3 elicited Ag-specific IgG but these responses were within error identical to those induced by SVLS alone without iNA (Fig. 2A and 2B), with p-values of 0.663 and 0.847 for pRBD3 on D5 and D11 and p-values of 0.728 and 0.787 on D5 and D11 for pHEL3 from one-way ANOVA tests. As we demonstrated previously (*15*), when provided in a simple admixture, these nucleic acids of all-natural phosphodiester backbones were quickly degraded in biological milieu. In contrast, when encapsulated within SVLS, the lipid bilayer structures protected iNA from nuclease degradation. As a consequence, even nucleic acids of all-natural phosphodiester backbones can unleash potent activity in current setting, when delivered together with ED on the same structures. These results are overall consistent with prior observations that simultaneous presence on the same particulate antigens foster the synergy between ED and nucleic acids on Ag-specific B cells (*56*, *57*).

Strikingly, we noticed that as low as a few molecules of Ag per SVLS were able to elicit these strong responses for both pRBD(DNA1) and pHEL(DNA1) (Fig. 3A-3D, Condition 4). These results are surprising because an ED less than 20 was not sufficient to elicit an Ag-specific IgG above background for either pRBD or pHEL without iNA (Fig. 2). These data thus reveal that it is the integrative signals from both ED and iNA *on individual SVLS* that set the threshold for the induction of IgG *in vivo*. This integrative signal required for IgG

bioRxiv preprint doi: https://doi.org/10.1101/2023.02.20.529089; this version posted February 21, 2023. The copyright holder for this preprint (which was not certified by peer review) is the author/funder. All rights reserved. No reuse allowed without permission.

secretion can be achieved with ED alone, at the expense of a relatively high ED value (Conditions 6 and 7 in Fig. 2), or the collective signals from ED and iNA together.

The synergy between ED and iNA as we described above was also observed for two other nucleic acids that we tested: DNA2 and RNA1 (Fig. 3A and 3C Condition 10 and 11). DNA2 is a 20-mer single-stranded DNA that harbors two unmethylated GpC dinucleotides but has all-natural phosphodiester backbone, which was usually used as a control for CpG-containing DNA. RNA1 is a 20-mer single-stranded RNA that is highly conserved among SARS-CoV-1, SARS-CoV-2 and MERS-CoV, and encodes motif V of an essential RNA helicase in these coronaviruses (*58*) (Materials and Methods). Although the IgG response from pRBD(DNA2) or pHEL(DNA2) was weaker than that of pRBD(DNA1) or pHEL(DNA1) at similar ED, the presence of the CpG dinucleotide motif was not required to observe this synergy. For pRBD(DNA2), the responses on both D5 and D11 were significantly higher than those induced by pRBD3, an SVLS of similar ED but without iNA (Fig. 2A Condition 6), with p-values of 0.0104 and 3.76e-4 from one-way ANOVA tests. For pHEL(DNA2), the responses on both D5 and D11 were also significantly higher than those induced by pHEL3, an SVLS of even higher ED but without iNA (Fig. 2B Condition 6), with p-values of 0.0494 and 0.0285 from one-way ANOVA tests. For pRBD(RNA1) (Fig. 3B Condition 11), although the IgG titer on D5 was lower than that induced by pRBD(DNA1)4, an SVLS of similar ED with DNA1 (Fig. 3B Condition 7, p-value=2.88e-8 from one-way ANOVA test), the IgG titer on D11 was statistically identical (p-value=0.356 from one-way ANOVA test). Therefore, CpG DNA is not unique in its strong potency for the synergistic induction of Ag-specific IgG responses. A natural viral genomic sequence is sufficient to induce a strong and rapid IgG response that is comparable in its magnitude.

bioRxiv preprint doi: https://doi.org/10.1101/2023.02.20.529089; this version posted February 21, 2023. The copyright holder for this preprint (which was not certified by peer review) is the author/funder. All rights reserved. No reuse allowed without permission.

The use of B6 mice allows us to test several genetic conditions for mechanisms behind the enormous synergy between ED and iNA. First, the synergy was largely T-cell independent, as shown by the strong Ag-specific IgG observed in T-deficient mice for pRBD(DNA1) and pRBD(RNA1) (Fig. 3A-3B, Condition 8 and 12), pHEL(DNA1) and pHEL(RNA1) (Fig. 3C-3D, Condition 8 and 12). In contrast, the strong synergy required MyD88 or Toll-like receptors, as shown by the much attenuated IgG in mice deficient in MyD88 for pRBD(DNA1) or pHEL(DNA1) (Fig. 3A and 3C, Condition 9); and in mice deficient in Toll-like receptor 7 for pRBD(RNA1) or pHEL(RNA1) (Fig. 3A and 3C, Condition 13). However, in mice deficient in CD19, strikingly, the presence of DNA1 internal to these SVLS can elicit a fast and strong IgG response as early as D5 for both pRBD(DNA1) and pHEL(DNA1) (Fig. 3A and 3C, Condition 14, circles). On D11, the IgG titer induced by pRBD(DNA1)4 in CD19$^{-/-}$ mice (Fig. 3B Condition 14) was as strong as that in wtB6 mice induced by the same agent at the same Ag dose (Fig. 3B Condition 7, p-value=0.356 from one-way ANOVA test). Likewise, the IgG titer induced by pHEL(DNA1)2 in CD19$^{-/-}$ mice on D11 (Fig. 3D Condition 14) was statistically identical to that in wtB6 mice induced by the same agent at the same Ag dose (Fig. 3D Condition 5, p-value=0.537 from one-way ANOVA test). These results are in sharp contrast to the requirement of CD19 by either pRBD or pHEL for induction of IgG in the absence of iNA (Fig. 2A-2B, Condition 10), and reveal that the synergistic signal co-delivered by ED and iNA for B cell activation can be strong enough to activate Ag-specific B cells even in the absence of the coreceptor CD19. Independent of the results from Condition 4 in wtB6 mice (Fig. 3A and 3C), these results in CD19$^{-/-}$ mice once again demonstrate that it is the integrative signals from ED and iNA together *on individual SVLS* that set the threshold for the induction of Ag-specific IgG *in vivo*.

bioRxiv preprint doi: https://doi.org/10.1101/2023.02.20.529089; this version posted February 21, 2023. The copyright holder for this preprint (which was not certified by peer review) is the author/funder. All rights reserved. No reuse allowed without permission.

We also compared the Ab responses induced by SVLS with iNA (SVLS(iNA) herein) to a commonly used bacteriophage VLP-based vaccine platform (*17, 18*). The strong IgG induced by SVLS(iNA) was comparable in titers to those elicited by RBD or HEL conjugated on bacteriophage Qβ VLPs at the same Ag dose, despite the complete absence of the bacteriophage Qβ coat proteins in these SVLS(iNA). This was shown by Condition 15 in Fig. 3A and 3B for a Qβ-RBD conjugate with an ED of 200 and Condition 15 in Fig 3C and 3D for a Qβ-HEL conjugate with an ED of 10 in wtB6. One-way ANOVA tests on these titer values revealed that Qβ-RBD induced the same level of RBD-specific IgG titers on D5 as pRBD(DNA1)1 and pRBD(DNA1)2, which were lower than those for pRBD(DNA1)3 and pRBD(DNA1)4; and Qβ-RBD induced the same level of RBD-specific IgG titers on D11 as pRBD(DNA1)3 and pRBD(DNA1)4, which were higher than those for pRBD(DNA1)1 and pRBD(DNA1)2 (Table S2A). For HEL, Qβ-HEL induced the same level of HEL-specific IgG titers on D5 and D11 as all pHEL(DNA1) (Table S2B). These results suggest that it is possible to elicit IgG responses of a similar magnitude to bacteriophage VLPs using highly purified components.

Can these IgG molecules neutralize cognate viral infectivity? As shown in Fig. 3E (Conditions 4-7, 10-11, the same set of conditions as in Fig. 3A), the strong IgG induced by pRBD(iNA) as early as D5 after injection can potently neutralize HIV-1 pseudovirions that display the cognate S protein of SARS-CoV-2 *in vitro*, with an even stronger potency on D11 after immunization. These strong neutralizing activities were obtained for all iNA sequences that we tested, suggesting a broad relevance of these results to understanding viral immunogenicity. We noted that even in the absence of T cells, this nAb response was strong enough to potently neutralize cognate virions in vitro (Conditions 8 and 12 in Fig. 3E). These results are fully consistent with live viral infection literature showing potent nAb response in

bioRxiv preprint doi: https://doi.org/10.1101/2023.02.20.529089; this version posted February 21, 2023. The copyright holder for this preprint (which was not certified by peer review) is the author/funder. All rights reserved. No reuse allowed without permission.

the absence of $CD4^+$ T cells (*6-10*). Yet the data herein reveal that live infection is not required to mount a fast and potent nAb response; all that is needed are the key *external* signals common to viral infection: ED and iNA. This fast and potent nAb response was also mounted in $CD19^{-/-}$ mice (Condition 14 in Fig. 3E), confirming that it is the integrative signals from ED and iNA *on individual SVLS* that matters. Once the ED and iNA signals are strong enough, the coreceptor CD19 is not required for a potent nAb response.

Like we observed in the B6 background, strong and fast IgG responses were also induced by SVLS(iNA) in BALB/c mice as early as D5. As shown in Fig. 3F, BALB/c mice mounted strong IgG responses towards pRBD(DNA1) of varied ED (Fig. 3F left, Conditions 4-7) with comparable magnitudes to B6 on both D5 and D11. Likely due to the available T cell help in BALB/c mice for HEL, the IgG responses towards pHEL(DNA1) of varied ED in BALB/c mice were even stronger on D11 than those in wtB6 (Fig. 3F right, Conditions 5-7), indicated by one-way ANOVA tests on these titer values (Table S3). Therefore, a nAb response was robustly initiated upon a single exposure to a submicrogram dose of Ag on SVLS(iNA) in the absence of any other adjuvants in both strains of mice. The similar magnitudes of these responses between B6 and BALB/c mice suggest that this rapid and strong IgG secretion in response to the combined signals from ED and iNA is conserved between the two strains and is highly potent against pseudovirions even in the absence of T cell help (Fig. 3, Conditions 8 and 12). In fact, these two signals, ED and iNA, are commonly found in virtually all viruses. Moreover, for both RBD and HEL, these responses induced by SVLS(iNA) could be quantitatively compared to those induced by either Qβ-RBD (Fig. 3F left, Condition 15) or Qβ-HEL conjugate (Fig. 3F right, Condition 15) at the same Ag dose in BALB/c mice. Comparison with bacteriophage Qβ VLPs revealed that only three biochemical ingredients

bioRxiv preprint doi: https://doi.org/10.1101/2023.02.20.529089; this version posted February 21, 2023. The copyright holder for this preprint (which was not certified by peer review) is the author/funder. All rights reserved. No reuse allowed without permission.

are needed to reconstitute such a response of similar magnitude: one foreign protein, iNA and lipids.

For both pRBD(iNA) and pHEL(iNA) in wtB6, the strong IgG response induced IgG1, IgG2b, IgG2c and IgG3, with IgG2c being the dominant subclass for almost all the SVLS(iNA) (Fig. 3G through 3N). Analogous to wtB6, the IgG response in BALB/c induced IgG1, IgG2a, IgG2b, and IgG3, with IgG2a being the dominant subclass (Fig. S5) (*59*). All iNA, including DNA1, DNA2 and RNA1, induced IgG2c in B6 genetic background (Fig. 3I and 3M), which was in sharp contrast to the undetectable IgG2c upon pRBD or pHEL immunization without iNA (Fig. S2B and S2D). Therefore these SVLS(iNA) can induce all the IgG subclasses known in mice, in the absence of live infection or any other adjuvants. Notably, incorporation of iNA lowers the ED thresholds for each IgG subclass. For SVLS without iNA, BALB/c mice mounted a stronger IgG1 response than wtB6 on D11 (Fig. S3). With iNA, the level of IgG1 is now comparable between the two strains particularly for RBD on both D5 and D11 (Fig. 3G, Fig. S5A and Table S4 for one-way ANOVA tests). Moreover, the comparison between SVLS(iNA) and Qβ-conjugated Ags reveals that Qβ was a stronger inducer of IgG1 after D5 of immunization in both wtB6 (Fig. 3G and 3K, Condition 15) and BALB/c mice (Fig. S5A and S5E, Condition 6), although IgG1 is not the dominant IgG subclass induced by SVLS(iNA). One possibility among others for this difference is the presence of multiple copies of the bacteriophage coat protein in Qβ VLPs, a foreign protein that is known to recruit T cell help in wtB6 (*14*). Compared to the strong Ag-specific IgG response, the IgM response induced by the SVLS(iNA) or Qβ conjugates remained low overall in both B6 and BALB/c mice and dropped substantially on D11 for both RBD and HEL-conjugated Ags. (Fig. S6).

bioRxiv preprint doi: https://doi.org/10.1101/2023.02.20.529089; this version posted February 21, 2023. The copyright holder for this preprint (which was not certified by peer review) is the author/funder. All rights reserved. No reuse allowed without permission.

How long will the strong Ag-specific IgG last from a single exposure to the Ags at submicrogram dose in the absence of any other adjuvants? In a typical live viral infection, the durability of the antibody response has been well documented (*5*) and, in humans, can range from 3 months to 75 years. We found that the durability of the Ag-specific IgG upon a single exposure to SVLS varies strongly depending on the host strain of the animals. As shown in Fig. 4A, the RBD-specific IgG in wtB6 mice elicited by pRBD(DNA1) peaked around 2 months after the exposure and then slowly decayed over the time span of one year (blue solid symbols). Without internal DNA1, the IgG response was at least 10-fold lower in magnitude (note the different sera dilution factors listed in figure inset), peaked around one month after exposure, and decayed almost to background level over the course of one year. In contrast, the same agents induced long-lasting IgG whose magnitudes increased with time in BALB/c mice, as shown in Fig. 4B. The growing trends were true for both pRBD and pRBD(DNA1), but the presence of DNA1 elicited much higher IgG levels. Despite the waning level of the RBD-specific IgG in wtB6 over time, sera collected over the one-year period remained highly effective in neutralization of cognate pseudovirions (grey symbols in Fig. 4C). Sera from immunized BALB/c mice collected over a year after immunization also had strong neutralizing activity (white symbols in Fig. 4C). All these neutralization activities came from just a single injection of pRBD(DNA1) at a submicrogram dose in the absence of any other adjuvants. The trends of Ag-specific IgG that varied with host animals were also observed for HEL-conjugated SVLS, as shown in Fig. 4D for wtB6 upon a single injection of pHEL(DNA1) or pHEL. For all cases in B6, the levels of HEL-specific IgG waned over time. It is worth noting that the peak values for HEL-specific IgG induced by pHEL(DNA1) (blue symbols in Fig. 4D) were much lower than those for RBD-specific IgG induced by pRBD(DNA1) (blue symbols in Fig. 4A), likely due to the absence of T cell help for HEL in wtB6. In contrast, both pHEL and pHEL(DNA1) induced long-lasting HEL-specific IgG that

bioRxiv preprint doi: https://doi.org/10.1101/2023.02.20.529089; this version posted February 21, 2023. The copyright holder for this preprint (which was not certified by peer review) is the author/funder. All rights reserved. No reuse allowed without permission.

grew with time in magnitudes in BALB/c mice (Fig. 4E), quantitatively similar to those trends for pRBD and pRBD(DNA1) in BALB/c mice (Fig. 4B). Also, with internal DNA1, the HEL-specific IgG was much stronger than those induced by pHEL without iNA over the one-year period, analogous to the situation induced by pRBD(DNA1) in comparison to pRBD in BALB/c mice over the same period of time. Therefore, despite similar magnitudes of the nAb responses initiated by SVLS(iNA) in wtB6 and BALB/c mice (Fig. 3B, 3D and 3F), differences in genetic backgrounds contributed substantially to the durability of the nAb response. The presence of iNA induced a stronger and more durable nAb response compared to SVLS without iNA. The durable IgG response from pHEL(DNA1) in B6 mice (Fig. 4D blue symbols) suggests that long-lived plasma cells may have been generated in the absence of cognate T cell help.

The rising response of IgG with time in BALB/c mice suggests affinity maturation upon a single injection of submicrogram dose of Ags in the absence of any other adjuvants. To examine these IgG responses in more detail, we conducted Ag-specific binding measurements using biolayer interferometry. First, the streptavidin sensor was coated with biotinylated Ag at a low density to ensure measurement of monovalent binding and dissociation by IgG, which was confirmed by comparing the rates of dissociation between a monoclonal mouse anti-RBD IgG and its Fab fragments (Fig. S7). Second, the sera from individual animals at different times post injection were subjected to binding and dissociation measurements in real time, as shown in Fig. 4F and Fig. 4G for sera from a BALB/c mouse immunized with pRBD(DNA1)3 and in Fig. 4H and Fig. 4I for sera from a BALB/c mouse immunized with pHEL(DNA1)1, respectively. The amplitudes from real-time binding and dissociation allowed us to calculate the percentages of Ag-specific IgG that remained bound at the end of dissociation (Fig. S8A and S8B), which is a direct indicator of antibody affinity

bioRxiv preprint doi: https://doi.org/10.1101/2023.02.20.529089; this version posted February 21, 2023. The copyright holder for this preprint (which was not certified by peer review) is the author/funder. All rights reserved. No reuse allowed without permission.

that is largely independent of their input concentrations (Fig. S8C). As shown in Fig. 4J, the percentages of Ag-specific IgG that remained bound at the end of dissociation showed a progressive increase until 2 months after the BALB/c mice were injected with either pRBD(DNA1) (red symbols) or pHEL(DNA1) (blue symbols), demonstrating affinity maturation. This was in sharp contrast to the sera from a B6 TCR$^{-/-}$ mouse that was injected with pHEL(DNA1)1 (green diamonds). Moreover, it is surprising to note that for all cases, regardless of the specific Ags, the off rates of the Ag-specific IgG induced by either pRBD(DNA1) or pHEL(DNA1) were already at $(5.2\pm0.3)\times10^{-4}$ s^{-1} on D5, including the TCR$^{-/-}$ mouse (green diamonds in Fig. 4K). These values of off rates were comparable to the off rate of $(3.9\pm0.3)\times10^{-4}$ s^{-1} measured for the commercial monoclonal IgG2a for RBD (Fig. S7E), which is shown as a dashed line in Fig. 4K. This commercial IgG2a can potently block the binding of RBD to human ACE2 at a concentration of 0.05-0.25 μg/mL (Biolegend CAT#944803). Over the 6-month period after a single injection, the off rates of the Ag-specific IgG from all these animals underwent little or no changes (Fig. 4K). Thus, the affinity maturation should mostly come from optimization of the IgG on rate (*60*).

To confirm this, we first determined the concentration of Ag-specific IgG using a biotinylated Ag pulldown assay with streptavidin-coated magnetic beads (S-beads) followed by quantitative western blotting. These results were shown in Fig. 4L for the capture of RBD-specific IgG on D11 and D123, respectively, from a BALB/c mouse immunized with a single injection of pRBD(DNA1)3 in the absence of any other adjuvants. To confirm complete capture of the RBD-specific IgG, we used increasing concentrations of biotin-RBD, as indicated on Lanes 2, 3 and 4 for D11 sera and Lanes 6, 7, and 8 for D123 sera. Comparison with a standard curve (Fig. S9) obtained from the same western blots yielded the concentration for all these samples as shown in the bottom of Fig. 4L. For D11 sera, Lanes 2,

bioRxiv preprint doi: https://doi.org/10.1101/2023.02.20.529089; this version posted February 21, 2023. The copyright holder for this preprint (which was not certified by peer review) is the author/funder. All rights reserved. No reuse allowed without permission.

3 and 4 yielded very similar concentrations, with an average of 0.139±0.007 mg/mL. A one-way ANOVA test among Lanes 2, 3, and 4 returned a p-value of 0.717; therefore, there were no statistically significant differences among these measurements with increasing biotin-RBD, which indicates that we captured nearly all RBD-specific IgG from D11 sera. For D123 sera, Lanes 6, 7 and 8 also yielded very similar concentrations, with an average of 0.356±0.007 mg/mL. A one-way ANOVA test among these lanes returned a p-value of 0.96, again demonstrating no statistically significant differences among these measurements with increasing biotin-RBD and indicating that we have captured nearly all RBD-specific IgG from D123 sera. However, a one-way ANOVA test between D11 and D123 measurements returned a p-value of 2.9e-5, indicating that the concentrations of RBD-specific IgG were significantly different in the sera from these two different dates. These concentrations allowed us to measure the on rates of RBD-specific IgG to RBD using biolayer interferometry by using serial dilutions of the respective sera, as shown in Fig. 4M for the series of binding curves from D11 sera and Fig. 4N for the series of binding curves from D123 sera. All these binding curves can be well described by exponential functions (solid black lines). We plotted the observed rate constants from these exponential fits as a function of the RBD-specific IgG molar concentration in Fig. 4O, which showed expected linear dependence for both D11 and D123 sera (straight red lines). The slopes of these lines determined the bi-molecular rate constants for the binding between RBD and RBD-specific IgG, which were $(4.2\pm0.2)\times10^{4}$ $M^{-1}s^{-1}$ on D11 and $(1.2\pm0.1)\times10^{5}$ $M^{-1}s^{-1}$ on D123. Therefore, the binding rate constants increased almost 3-fold as a result of affinity maturation from D11 to D123.

In summary, we discovered a strong and rapid IgG response in mice that can be triggered by only three biochemical ingredients that are commonly found in naturally occurring enveloped

bioRxiv preprint doi: https://doi.org/10.1101/2023.02.20.529089; this version posted February 21, 2023. The copyright holder for this preprint (which was not certified by peer review) is the author/funder. All rights reserved. No reuse allowed without permission.

viruses: a foreign protein, iNA and lipids. This response as observed for two completely unrelated protein Ags on SVLS with RNA or DNA of different sequences but all-natural phosphodiester backbones suggests a broad relevance of the current findings for understanding viral immunogenicity and the mechanisms of nAb responses. This IgG response is characterized by a fast onset of T-independent IgG of different subclasses, the ability to potently neutralize cognate virions, and depending on the mouse strain, affinity maturation together with a durable, long-lived response. This system recapitulates several key features of the nAb response to live viral infections and therefore suggests a common mechanism for their induction. Using a set of SVLS that we constructed with highly purified biochemical ingredients, we have identified the minimal set of external signals from a virion that can robustly initiate strong antiviral IgG responses *in vivo*. Biochemically, only two ingredients are required to initiate an IgG response. The oriented display of viral surface proteins above a threshold ED on a virion-sized sphere is sufficient to serve as a stand-alone 'danger' signal to trigger an IgG response in the absence of Toll-like receptor signalling. Consistent with this, *in vitro* studies using the same system of pHEL demonstrated that these SVLS without iNA could activate the NF-κB signalling pathway in Ag-specific B cells independently of MyD88, IRAK1/4 and CD40 ligation (*44*). Although the response *in vivo* towards this ED signal is weaker in B6 mice than BALB/c, in the presence of iNA, both mouse strains mounted strong nAb responses of comparable magnitudes, suggesting that this is an evolutionarily conserved mechanism. The speed together with the magnitude of this response is largely independent of T cells, affording the host with a mechanism of fast and strong nAb response that would be critical for antiviral defense. This mechanism explains the induction of protective nAbs observed in live viral infections that do not require somatic hypermutation or affinity maturation (*61*). In current study, this nAb response was initiated by SVLS at submicrogram Ag dose (picomoles of particles) upon a single exposure to the

bioRxiv preprint doi: https://doi.org/10.1101/2023.02.20.529089; this version posted February 21, 2023. The copyright holder for this preprint (which was not certified by peer review) is the author/funder. All rights reserved. No reuse allowed without permission.

animal host in the absence of any other adjuvants. In the absence of iNA, the oriented display of proteins above a threshold ED on a virion-sized sphere can induce IgG1, IgG2b and IgG3 in both wtB6 and BALB/c mice. In the presence of iNA, IgG2a/2c was also induced. Thus, neither live infection nor any other adjuvants are necessary to initiate these class switches. B cells use a signalling mechanism that is distinct from that for soluble antigens to sense these structures, notably through evasion of Lyn-dependent inhibitory pathways to initiate proliferation (*44*). CD19 is an important coreceptor for B cell antigen receptor activation (*52-54*). Although CD19 is required for a nAb response *in vivo* in the absence of iNA, in the presence of iNA, the integrative signals from both ED and iNA *on individual SVLS* can be strong enough to overcome the requirement for CD19. The data in the current study suggest that this mechanism for the initiation of a nAb response is conserved between two different strains of mice: wtB6 and BALB/c. However, the duration of this initial nAb response differs substantially between the two strains, suggesting the involvement of host genetic factors in modulating the durability of this important response. For decades, the highly repetitive display of viral surface antigens was viewed as the distinct 'viral' signal for activation of B cells (*62*). This current study shows that B cells integrate signals from both B cell antigen receptors and Toll-like receptors collected from individual particulate Ags to initiate a nAb response in the absence of cognate T cell help. High ED is necessary to initiate this response in the absence of effective iNA signals. However, in the presence of iNA, as low as a few molecules of surface Ag can trigger an immediate and strong IgG response. Therefore, high ED by a bona fide virus is capable but not required to initiate this response. It is remarkable that the Ag-specific IgG elicited by these SVLS has slow off rates that are less than 0.001 s^{-1}, as early as Day 5 post Ag exposure, regardless of the specific protein Ag or the mice strains and even in the absence of functional T cells (Fig. 4K). We hypothesize that this is at evolutionary advantage of the host because defects in IgG

bioRxiv preprint doi: https://doi.org/10.1101/2023.02.20.529089; this version posted February 21, 2023. The copyright holder for this preprint (which was not certified by peer review) is the author/funder. All rights reserved. No reuse allowed without permission.

on rate can be potentially compensated by a high concentration of the IgG secreted in response to acute viral infection. This suggests that upon germinal center formation in a suitable host, the major improvements to these nAbs are likely in the on rates of Ag binding (*63*), which has been suggested by human nAbs directed towards respiratory syncytial virus (*60*). It's important to note that, in addition to binding rates, an IgG's potency for neutralizing viral infectivity is also influenced by the virus' ED. Specifically, the ED of the virus can impact the stability and effectiveness of bivalent binding by the IgG, which is more effective than monovalent binding (*36, 64*). Table S5 summarizes the mechanisms of nAb response from current studies together with their implications for understanding of viral immunogenicity. Lastly, the potency of the IgG response triggered by these SVLS can be compared to that of well-established bacteriophage VLPs, suggesting that the immunogenicity of VLPs may be reconstituted using highly purified components. The completely synthetic nature of these SVLS may be useful for vaccine design and formulation, and the use of nucleic acids with native phosphodiester backbones without the need for nuclease-resistant phosphorothioate could substantially reduce the cost of vaccine manufacture.

bioRxiv preprint doi: https://doi.org/10.1101/2023.02.20.529089; this version posted February 21, 2023. The copyright holder for this preprint (which was not certified by peer review) is the author/funder. All rights reserved. No reuse allowed without permission.

MATERIALS AND METHODS

Synthesis of SVLS

All SVLS used throughout this study were prepared following protocols we published previously (*14-16*). These SVLS were constructed using nonimmunogenic lipids, with phosphatidylcholine and cholesterol comprising ≥ 99% of all lipids. These structures display protein antigens (Ags) of choice in a specific orientation on their surfaces with a regulated ED that quantitatively mimics the surface of naturally occurring viruses (*36, 37*) (Fig. 1). The HEL recombinant protein used in this study contains two site-directed mutations at R73E and D101R and was overexpressed in *E. coli* and purified to >95% purity following our established protocols (*15*). The SARS-CoV-2 RBD recombinant protein used in this study was overexpressed using 293F cells and also purified to >95% purity following our established protocols (*16*). DNA1, DNA2 and RNA1 were custom synthesized by IDT. The sequence of DNA1 is as follows, 5'-TCCATGA<u>CG</u>TTCCTGA<u>CG</u>TT-3'. The sequence of DNA2 is as follows, 5'-TCCATGA<u>GC</u>TTCCTGA<u>GC</u>TT-3'. The sequence of RNA1 is as follows, 5'-ACUGUUGAUUCAUCACAGGG-3'. Epitope density (ED) was quantified using methods that we established previously (*14-16, 33*) that were also validated by single-molecule fluorescence techniques (Fig. S1) that were developed and established in house (*34, 35*). For SVLS with iNA, the average number of internal nucleic acids (iNA) molecules per SVLS was also quantified using methods that we established previously (*15, 16*). Control SVLS had no surface protein conjugation nor internal encapsulated agents.

Conjugation of RBD or HEL to bacteriophage Qβ virus-like particles (VLPs)

bioRxiv preprint doi: https://doi.org/10.1101/2023.02.20.529089; this version posted February 21, 2023. The copyright holder for this preprint (which was not certified by peer review) is the author/funder. All rights reserved. No reuse allowed without permission.

The bacteriophage Qβ VLPs were prepared as described (*65*). The purified RBD or HEL recombinant proteins, which each contained a single reactive cysteine near their respective C-terminus, were conjugated to the surface of the VLPs using the heterobifunctional crosslinker Succinimidyl-6-[(β-maleimidopropionamido)hexanoate] (SMPH). Briefly, the VLPs were first derivatized with SMPH at a 10-fold molar excess of SMPH over Qβ coat protein. The mixture was incubated at 22°C for two hours and the excess crosslinker was removed by centrifugation at 4°C in an Amicon Ultra-4 centrifugal unit with a 100 kD cutoff. The RBD or HEL protein was then added to the derivatized VLPs and the mixture was incubated at 4°C overnight for RBD or at 20°C for 1 hour for HEL. Free proteins were then removed by centrifugation at 4°C in an Amicon Ultra-4 centrifugal unit with a 100 kD cutoff. The quantity of conjugated proteins was assessed using a denaturing polyacrylamide gel based on the intensity from silver staining in comparison with a standard curve obtained from the same gel.

Mice immunizations

All animal procedures were approved by the University of Michigan Animal Care and Use Committee. Female C57BL/6 or BALBc/J mice (8 weeks, Jackson Laboratory) were used for immunizations. Prior to inoculation, all injection samples were filtered through 0.45 µm pore size membrane to eliminate potential microbial contamination. 100 µL samples at a dose between 0.1 and 0.48 µg of respective protein Ags were injected into each mouse subcutaneously, 50 µL in each flank. Throughout the entire study, no adjuvants other than the SVLS were administered unless otherwise noted and only a single injection was administered throughout. Mouse blood was collected submentally using Microvette serum collection tubes (Sarstedt) three days before the first injection, and 5 days thereafter following specified blood collection schedules. The sera were harvested by centrifugation at 10,000 g for 5 minutes, aliquoted and immediately frozen and stored at -80°C.

bioRxiv preprint doi: https://doi.org/10.1101/2023.02.20.529089; this version posted February 21, 2023. The copyright holder for this preprint (which was not certified by peer review) is the author/funder. All rights reserved. No reuse allowed without permission.

Four strains of gene knockout mice were purchased from Jackson Laboratory: Tcrb^{tm1Mom}/ Tcrd^{tm1Mom} (#002122) (TCR$^{-/-}$ herein) was deficient in both alpha beta and gamma delta T-cell receptors (*48*). Myd88$^{tm1.Defr}$ (#009088) (MyD88$^{-/-}$ here in) encodes a deletion of exon 3 of the myeloid differentiation primary response gene 88 (*49*). Cd19$^{tm1(Cre)Cgn}$ (#006785) (CD19$^{-/-}$ herein) has a Cre recombinase gene inserted into the first exon of the CD19 gene thus abolishing CD19 gene function (*51*). Tlr7^{tm1Flv} (#008380) (TLR7$^{-/-}$ herein) has a segment of exon 3 of the Toll-like receptor 7 gene replaced by a lacZ gene and a loxP-flanked neomycin resistance cassette thus abolishing the function of Toll-like receptor 7 (*66*). Gene knockout mice were housed in a germ-free environment and immunization protocols were carried out as described above.

Enzyme-Linked Immunosorbent Assay (ELISA)

Blood serum was tested by ELISA in order to quantitate Ag-specific IgG responses to various immunizations. 96-well plates (Nunc MaxiSorp, Invitrogen) were coated overnight at 4°C with either 200 ng of sHEL or 320 ng of sRBD per well in PBS. After blocking with 1% Bovine Serum Albumin (BSA, Fisher) in PBS, mouse sera of specified dilution factors were added to each well for incubation at 22°C for 2 hours. After three washes using PBS with 0.05% Tween 20, secondary goat anti-mouse IgG Fc-HRP antibody (# 1033-05, Southern Biotech) was added in blocking buffer at 1:6000 dilution and incubated for 1 hour at 22°C. Following three washes, 100 µL of substrate 3,3',5,5'-Tetramethylbenzidine (Thermo Scientific) was added to each well and incubated in the dark for 10 minutes. The reaction was stopped by addition of 100 µL 2M sulfuric acid in each well. The optical density of each well at 450nm was measured using a microplate reader (Bio-Tek Synergy HT). All the OD

bioRxiv preprint doi: https://doi.org/10.1101/2023.02.20.529089; this version posted February 21, 2023. The copyright holder for this preprint (which was not certified by peer review) is the author/funder. All rights reserved. No reuse allowed without permission.

values reported were background subtracted by comparison between two wells that were coated with soluble protein and PBS, respectively. To determine the level of Ag-induced IgM in mice upon immunization by various agents, we used the following secondary antibody during ELISA: goat anti-mouse IgM HRP antibody (#1021-05, SouthernBiotech).

To determine the titers of Ag-specific IgG, we used a serial dilution of serum (from 1:100 dilution to 1:10,000,000 by a dilution factor of 10) for ELISA with the sHEL or sRBD protein. Cutoff values were calculated using the following equation as reported (*67*): Cutoff $= \bar{X} + SD \cdot f$, where $\bar{X}$ and SD are the mean and standard deviation of control well OD reading values, f is the standard deviation multiplier corresponding to different confidence levels. Specifically in our assays, f = 2.631 when the number of control wells was 4 and the confidence level was 95%. The titer value was determined as the highest dilution factor of the serum that still yielded an OD450 value higher than the above cutoff value in ELISA.

To determine the subclasses of IgG antibodies elicited in mice upon immunization by various agents, we used the following secondary antibodies during ELISA: goat anti-mouse IgG1 HRP antibody (#1071-05, SouthernBiotech), goat anti-mouse IgG2a HRP antibody (#1081-05, SouthernBiotech), goat anti-mouse IgG2b HRP antibody (#1091-05, SouthernBiotech), goat anti-mouse IgG2c HRP antibody (#1078-05, SouthernBiotech), and goat anti-mouse IgG3 HRP antibody (#1101-05, SouthernBiotech).

Preparation of HIV-1 virions pseudotyped with SARS-CoV-2 envelope

bioRxiv preprint doi: https://doi.org/10.1101/2023.02.20.529089; this version posted February 21, 2023. The copyright holder for this preprint (which was not certified by peer review) is the author/funder. All rights reserved. No reuse allowed without permission.

The HIV-1 pseudotyped with SARS-CoV-2 envelope was prepared following the published protocols (*68*) but with modifications. Briefly, HEK 293T/17 cells (ATCC, Manassas, VA) were cultured at 37°C with 5% CO_2 in DMEM supplemented with 10% FBS (HyClone Laboratories, Logan, UT). 10^6 293T cells in a 2-mL culture volume were seeded overnight in a 35-mm dish before transfection using the TransIT LT-1 transfection reagent (Mirus Bio, Madison, WI). For each dish, 2 μg of the provirus-containing plasmid pNL4-3 luc R^-E^- (*69*) (ARP-3418, NIH AIDS Research and Reference Reagent Program) was used to make the transfection reagent mixture, together with 1 μg of envelope expression plasmid pcDNA3.1 SARS-CoV-2 S D614G (*68*). The plasmid pcDNA3.1 SARS-CoV-2 S D614G was a gift from Jeremy Luban (Addgene plasmid # 158075 ; http://n2t.net/addgene:158075 ; RRID:Addgene_158075). The RBD amino acid sequence 328-537 encoded in this plasmid is identical to the sequence of RBD that we studied here. The transfection reagent mixture was incubated at room temperature for 15 min before drop wise addition to the culture medium, as we did previously (*70*). At 6 hours post transfection, the culture medium together with the transfection reagents was replaced with fresh complete medium and the incubation was continued at 37°C with 5% CO_2. At 48 hours post transfection, the entire culture medium containing single-cycle HIV-1 viruses was collected and filtered through a 0.45-μm syringe filter (Millex-HV PVDF, Millipore). The filtrate was then aliquoted on ice, flash-frozen in liquid nitrogen and stored in a -80°C freezer. The concentration of virion particles was quantitated using a HIV-1 p24 ELISA kit (CAT#XB-1000, XpressBio) as we described previously (*70*).

Virion neutralization assay

bioRxiv preprint doi: https://doi.org/10.1101/2023.02.20.529089; this version posted February 21, 2023. The copyright holder for this preprint (which was not certified by peer review) is the author/funder. All rights reserved. No reuse allowed without permission.

Virion neutralization assay follows the protocols we established previously but with important modifications (*70*). HIV-1 virions pseudotyped with SARS-CoV-2 envelope containing 9 ng of HIV-1 p24 were incubated with various mouse sera at 37°C for one hour, and then diluted with complete medium by 8-fold in volume for the sera to initiate infection of Huh-7.5 cells at 37°C for 2 hours. At the end of 2 hours, fresh medium was added to each well in a 24-well plate and the incubation was continued at 37°C with 5% CO_2. Luciferase activity was measured 48 hours after infection. Briefly, the culture medium was removed and replaced with 100 μL of complete medium. 100 μL of Bright-Glo™ reagent (CAT#E2610, Promega) that was just warmed to room temperature was then added to each well. The cells were incubated for three minutes at room temperature to allow cell lysis. After three minutes, 100 μL of lysate from each well was transferred to a single well in a 96-well black microtiter plate (Costar). Luminescence was measured using a Synergy™ HT multi-mode plate reader (BioTek Instruments Inc., Vermont) and background luminescence was subtracted using Huh-7.5 cells without virus infection. For comparison among different immunization groups in Fig. 2C and Fig. 3E, the luminescence readings for cells incubated with sera from PBS-injected mice was set as 100%. The luminescence readings from other groups were all normalized based on this and plotted as a percentage of remaining infectivity. For comparison among different time points post immunization in Fig. 4C, the luminescence readings for cells incubated with sera from each group of mice before injections was set as 100%. The luminescence readings from other time points for the same group were all normalized based on this and plotted as a percentage of remaining infectivity.

Flow cytometry analysis of mouse inguinal lymph nodes

bioRxiv preprint doi: https://doi.org/10.1101/2023.02.20.529089; this version posted February 21, 2023. The copyright holder for this preprint (which was not certified by peer review) is the author/funder. All rights reserved. No reuse allowed without permission.

On Day 12 following mouse inoculation with various agents, mice were euthanized by CO_2 inhalation followed by rapid dissection of the inguinal lymph nodes. The lymph nodes were minced on ice and a cellular suspension was separated from tissue using a 40 µm cell strainer. Single cell suspensions of mouse lymph node cells were first incubated with rat anti-mouse CD16/CD32 (BD Pharmingen #553142) on ice for 15 min, followed by incubation with fluorophore-conjugated antibodies on ice covered by aluminum foil. The cells were washed twice with 200 µL of FACS buffer, resuspended in FACS buffer, and fixed in the presence of 2% PFA at 22°C for 1 hour before data acquisition on a Miltenyi MACSQuant VYB flow cytometer equipped with 3 spatially-separated lasers (405, 488 and 561 nm) and 10 detection channels. A minimum of 100,000 events were collected for all experiments. The fluorophore-conjugated antibodies were pacific blue rat anti-mouse CD19 (Biolegend #115526), FITC rat anti-mouse GL7 antigen (Biolegend #144603), PE anti-mouse CD38 (Biolegend #102707), and APC anti-mouse CD95 (Biolegend #152603). The data were analyzed using FlowJo (BD).

BioLayer interferometry measurements

Affinity maturation of Ag-specific antibodies in animal sera together with binding and dissociation rate constants were measured using BioLayer interferometry. Briefly, the streptavidin sensor (Sartorius Corp) was coated with 50 nM RBD or HEL in 1×PBS for 30 min at 20°C, which was followed by washing in PBS for 10 min. For this application, both RBD and HEL were site-specifically biotinylated in house using EZ-link maleimide-PEG2-biotin (ThermoFisher, CAT#A39261). After sensor loading, they were dipped into antibodies or sera of varied dilutions in Buffer 1 to measure the binding in real time using an OctetRed BioLayer Interferometer equipped with 8 sensor positions that were read simultaneously. The measurement for binding was continued

bioRxiv preprint doi: https://doi.org/10.1101/2023.02.20.529089; this version posted February 21, 2023. The copyright holder for this preprint (which was not certified by peer review) is the author/funder. All rights reserved. No reuse allowed without permission.

for the indicated time, which was followed by dipping the sensors into Buffer 1 for the indicated time to monitor the dissociation in real time. Throughout, the measurements were done at 20°C. A PBS coated sensor control was included and subtracted from all the kinetic data before quantitative analysis. Buffer 1 was 1×PBS with 0.05% Tween 20 and 0.1% BSA. The percentage of IgG remaining bound, p, was determined by using the amplitude information from both binding and dissociation curves, specifically as follows, p=(A1+A2)/A1*100%, in which A1, a positive number, is the final amplitude at the end of binding measurement, and A2, a negative number as the result of dissociation, is the final amplitude at the end of dissociation measurement, as illustrated in Fig. S8A and S8B. In current study, most binding and dissociation events were measured continuously in real time for 50 min each. For experiments shown in Fig. 4M, the binding and dissociation were monitored continuously for 4000 s for better definition of the rate constants.

Measurement of Ag-specific IgG concentration in animal sera

We measured the concentration of Ag-specific IgG in the sera of immunized animals using streptavidin-coated magnetic beads. Specifically, high capacity Magne streptavidin beads (Promega CAT#V7820) were first exchanged into PBS buffer, and then mixed with biotinylated RBD or HEL for binding at 20°C for 1 hr with constant mixing on a lab vortexer. After this, the beads were washed 3 times using Buffer 1 and then mixed with sera also diluted in Buffer 1. The binding was continued at 20°C for 2 hrs with constant mixing. Finally, the supernatant was removed, and the bound IgG was resuspended in nonreducing Laemmli sample buffer at 95°C for 10 min. The amount of Ag-specific IgG was then quantitated by running a western blot using mouse IgG (Biolegend CAT#944803) of known mass as a standard. The secondary antibody used was goat anti-mouse IgG (Fc specific) conjugated with alkaline phosphatase from Sigma (CAT#A1418) and used at 1:3000 dilution.

bioRxiv preprint doi: https://doi.org/10.1101/2023.02.20.529089; this version posted February 21, 2023. The copyright holder for this preprint (which was not certified by peer review) is the author/funder. All rights reserved. No reuse allowed without permission.

Statistical analysis

Statistical analysis was carried out using the Statistics toolbox in MATLAB (Mathworks, MA). A comparison of two independent variables was carried out using a two-sample T-test. Data sets with more than two independent variables were analyzed using a one-way analysis of variance as indicated. P-values less than 0.05 were considered statistically significant. Throughout, all data points in figures were reported as mean ± standard error unless otherwise noted.

bioRxiv preprint doi: https://doi.org/10.1101/2023.02.20.529089; this version posted February 21, 2023. The copyright holder for this preprint (which was not certified by peer review) is the author/funder. All rights reserved. No reuse allowed without permission.

ACKNOWLEDGEMENTS

This work was supported by an NIH/NIAID grant (1R01AI155653-01A1) to WC and JZ. We thank Prof. Irina Grigorova for critical reading of the work during the early development of the manuscript. We thank Dr. Charlie Rice at Rockefeller University for the kind gift of Huh-7.5 cells. The following reagent was obtained through the AIDS Research and Reference Reagent Program, Division of AIDS, National Institute of Allergy and Infectious Diseases (NIAID), National Institutes of Health (NIH): pNL4-3.Luc.R-E- from Dr. Nathaniel Landau.

CONFLICT OF INTEREST

W. Cheng has a patent pending on SVLS. B. Chackerian has equity in Flagship Laboratories 72. J. Zikherman is on the scientific advisory board for Walking Fish Therapeutics. No other disclosures were reported.

bioRxiv preprint doi: https://doi.org/10.1101/2023.02.20.529089; this version posted February 21, 2023. The copyright holder for this preprint (which was not certified by peer review) is the author/funder. All rights reserved. No reuse allowed without permission.

Figures

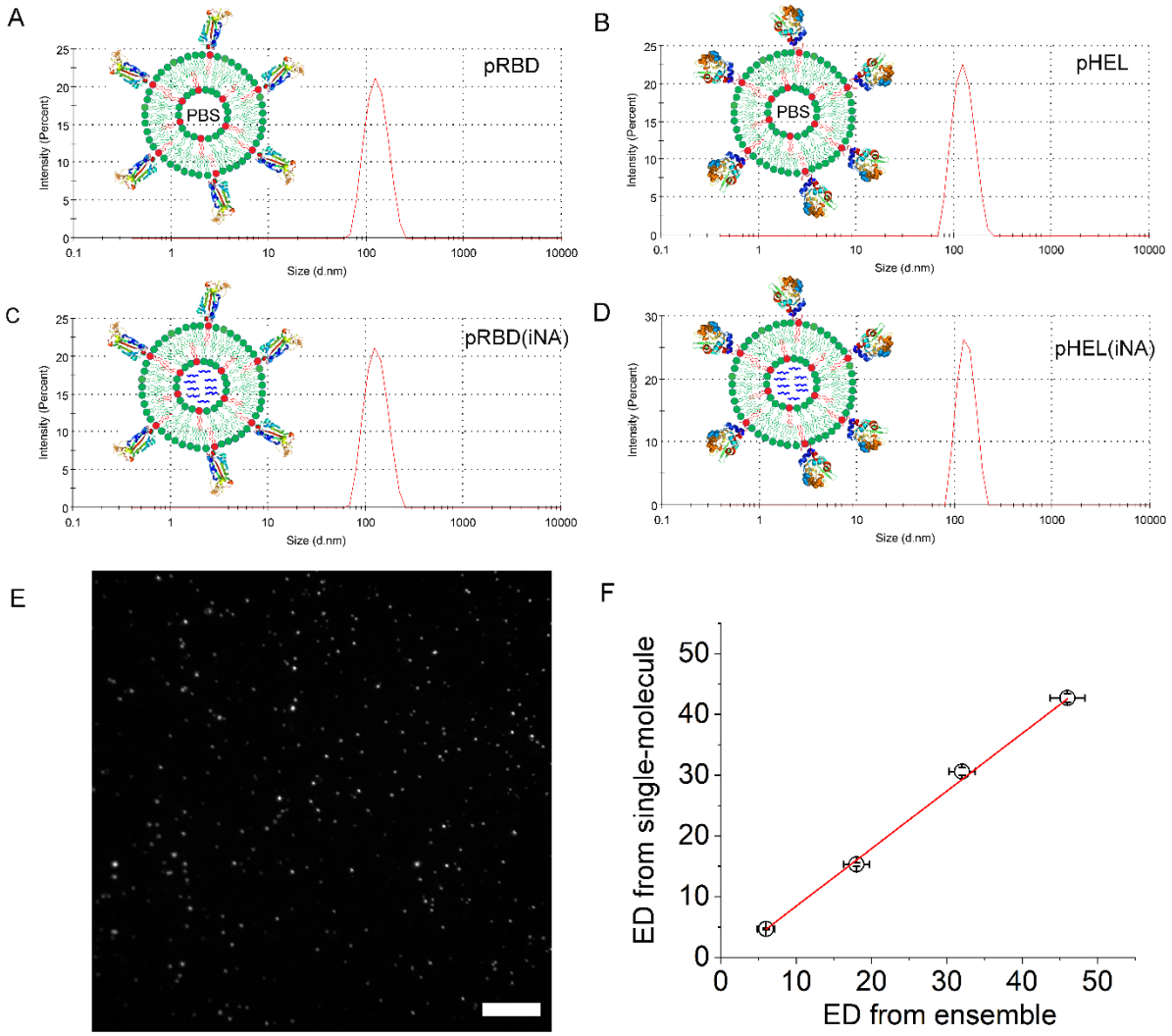

Fig. 1. Characterization of SVLS that quantitatively incorporate the common consensus features of enveloped viruses. (**A**) through (**D**): representative intensity distributions of particle sizes measured using dynamic light scattering for four types of SVLS, schematically shown as insets in each panel. The structure surface is conjugated with RBD (A, C) or HEL (B, D) site-specifically at regulated average spatial densities. The internal space of the structures is either PBS for investigation of ED in isolation (A, B) or loaded with nucleic acids to study the effects of iNA (C, D). The average diameters together with PDI values are 122 nm, 0.037 for a pRBD; 120 nm, 0.039 for a pHEL; 123 nm, 0.042 for a pRBD(DNA1); and 124 nm, 0.054 for a pHEL(DNA1). Cartoon insets adapted from (*15*, *16*). (**E**) A representative epi-fluorescence image of individual SVLS on poly-L-lysine coated coverslip stained by a fluorescent Fab (Fig. S1). The scale bar represents 10 µm. (**F**) Correlation between ED measured using single-molecule fluorescence technique (Fig. S1) and ensemble technique for a set of pRBD(DNA1).

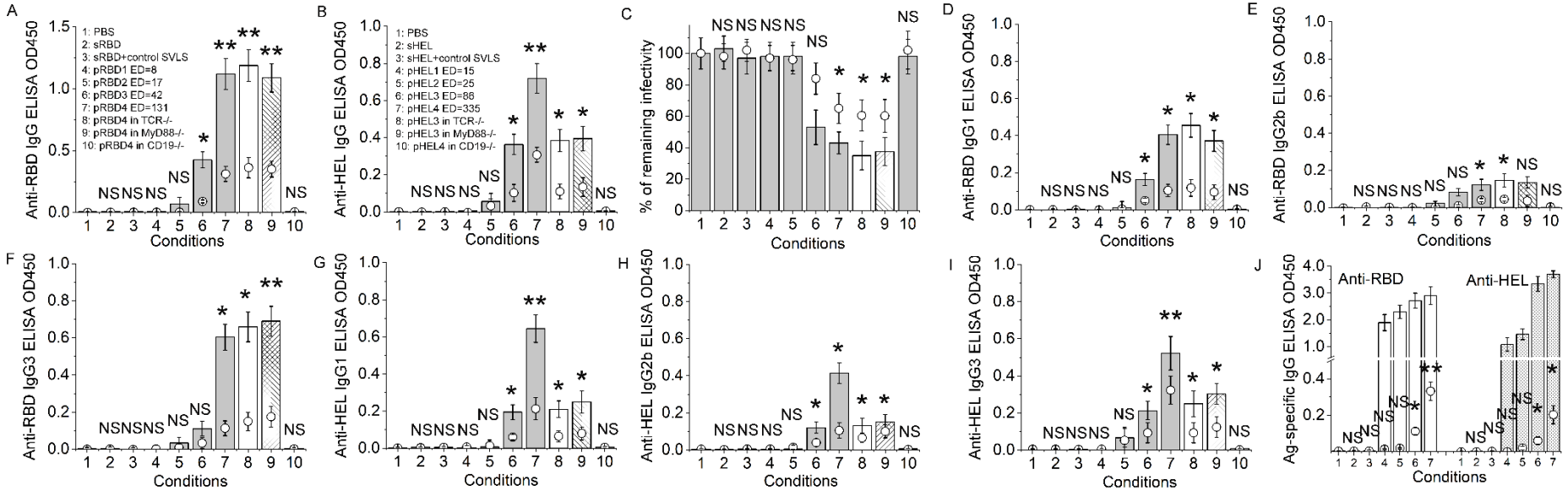

Fig. 2. Rapid nAb responses induced by SVLS without iNA. (**A**)(**B**) ELISA OD values for RBD-specific IgG (A) or HEL-specific IgG (B) in B6 genetic background after a single injection using various agents listed in the insets. (**C**) Neutralization of HIV-1 virions pseudotyped with SARS-CoV-2 S protein by mouse sera. (**D**) through (**I**): ELISA OD values for RBD- and HEL-specific IgG subclasses in (A) and (B). (**J**) ELISA OD values for RBD-specific IgG (left) or HEL-specific IgG (right) in BALB/c after a single injection using various agents listed in (A) and (B) insets. Throughout Fig. 2, data from D5 post immunization shown in circles and D11 shown in columns; sera were diluted 100-fold for all ELISA; the doses of RBD and HEL were 0.24 and 0.3 µg per animal, respectively for Conditions 2 through 10. The pairwise statistical difference between each condition and Condition 1 on Day 5 was determined by Student's T-test and shown using the following set of symbols; **: p-value < 0.01; *: p-value < 0.05; NS: not significant, p-value > 0.05. N=4.

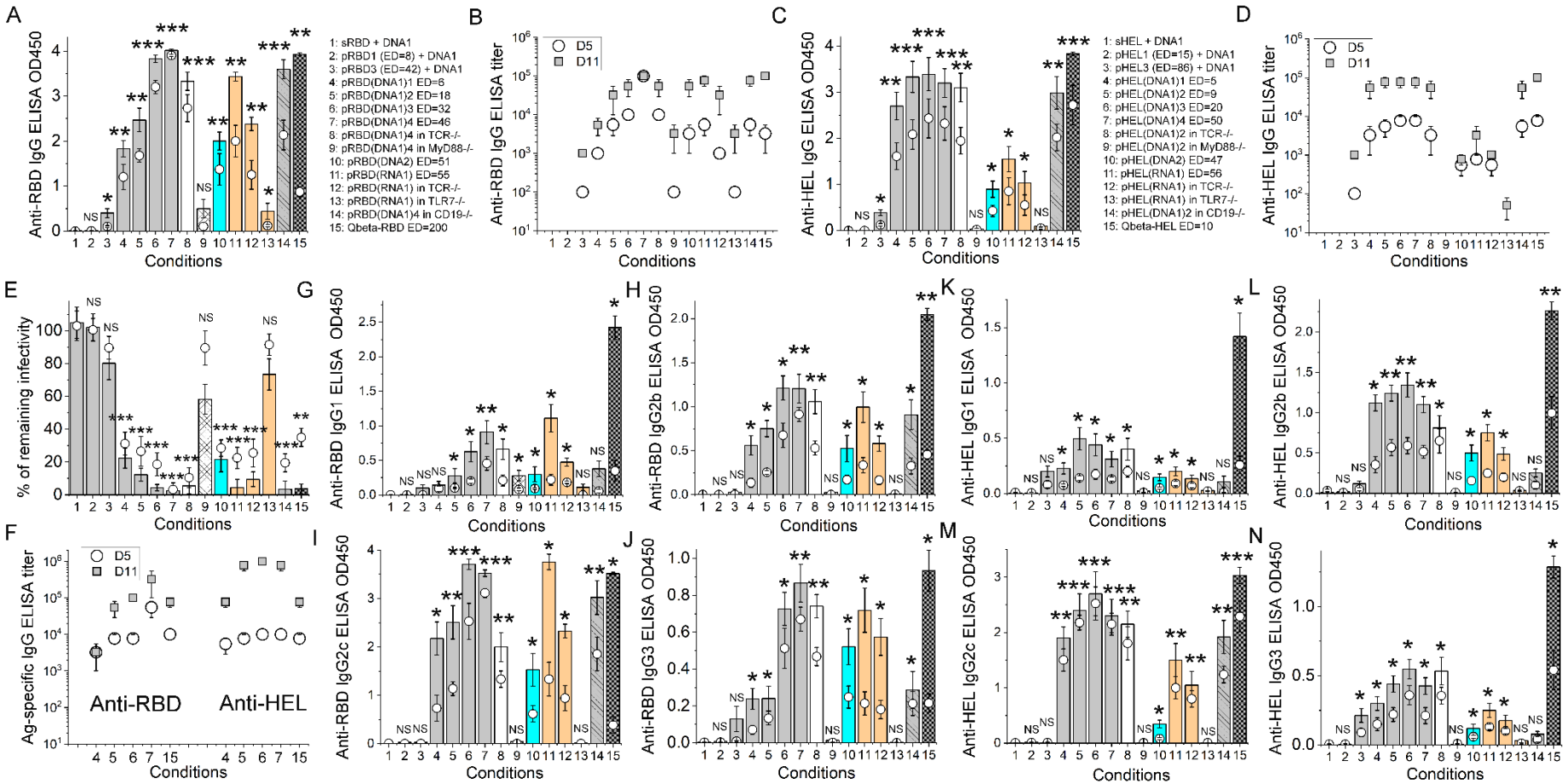

Fig. 3. Rapid nAb responses induced by SVLS with various iNA. (**A**) and (**C**) ELISA OD values for RBD-specific IgG (A) or HEL-specific IgG (C) in B6 genetic background after a single injection using various agents listed in the insets. (**B**) and (**D**) Titers for RBD-specific IgG (B) or HEL-specific IgG (D) measured for various conditions as in (A) and (C). (**E**) Neutralization of HIV-1 virions pseudotyped with SARS-CoV-2 S protein by mouse sera from various conditions in (A). (**F**) Ag-specific titer values for RBD-specific IgG (left) or HEL-specific IgG (right) in BALB/c after a single injection using agents #4, 5, 6, 7 and 15 as listed in (A) and (C) insets. (**G**) through (**N**): ELISA OD values for RBD-specific (G through J) and HEL-specific (K through N) IgG subclasses for sera from (A) and (C), respectively. Throughout Fig. 3, data from D5

post immunization shown in circles and D11 shown in columns or squares; sera were diluted 100-fold for all ELISA except titers; the doses of RBD and HEL were 0.24 and 0.1 µg per animal, respectively for Conditions 2 through 15; the pairwise statistical difference between each condition and Condition 1 on Day 5 was determined by Student's T-test and shown using the following set of symbols; ***: p-value < 0.001; **: p-value < 0.01; *: p-value < 0.05; NS: not significant, p-value > 0.05. N=4.

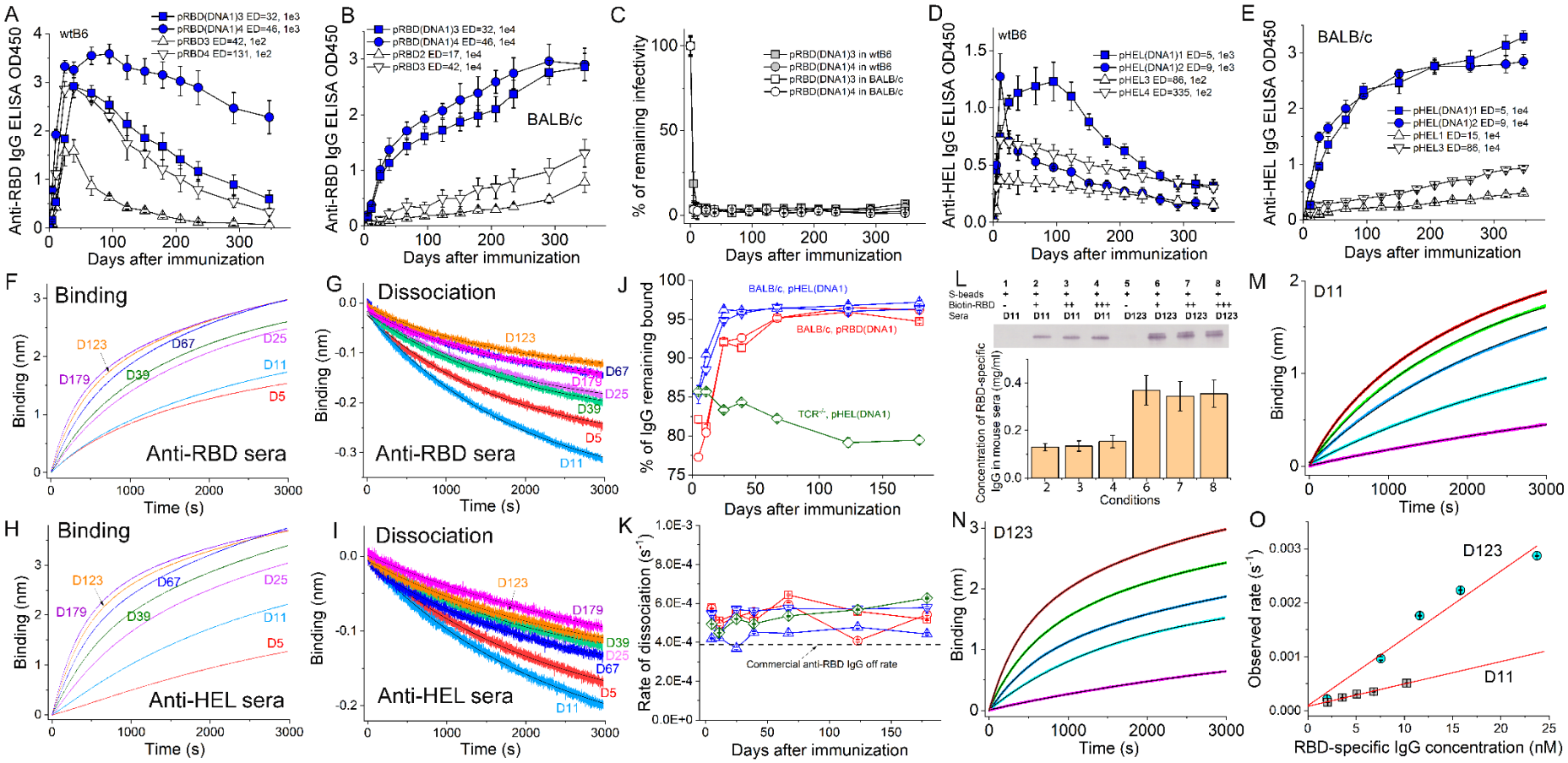

Fig. 4. Duration and affinity maturation of the nAb response induced by SVLS. (**A**)(**B**) and (**D**)(**E**) Time courses of ELISA OD450 values for Ag-specific IgG measured from mouse sera collected on different days after a single injection of various agents listed in each inset, together with respective sera dilutions. (**C**) Time courses of pseudovirion neutralization by various sera from immunized animals as listed in the inset. (**F**)(**G**)(**H**) and (**I**) Real-time binding and dissociation measurements for mouse sera from different days after immunization using BioLayer interferometry. (**J**)(**K**), percent of IgG remaining bound at the end of dissociation (J) and the dissociation rates (K) as a function of days after immunization measured from BioLayer interferometry. Red squares, red circles, upper triangles, down triangles and diamonds are for pRBD(DNA1)3, pRBD(DNA1)4, pHEL(DNA1)1, pHEL(DNA1)2, and pHEL(DNA1)1 respectively. (**L**) RBD-specific IgG capture using

streptavidin-coated magnetic beads together with biotin-RBD. (**M**)(**N**) Real-time binding curves for mouse sera to biotin-RBD at various dilutions from D11 and D123. (**O**) The observed binding rate constants as a function of measured RBD-specific IgG concentration. The dose of Ags were the same as indicated in Fig. 3 legend.

bioRxiv preprint doi: https://doi.org/10.1101/2023.02.20.529089; this version posted February 21, 2023. The copyright holder for this preprint (which was not certified by peer review) is the author/funder. All rights reserved. No reuse allowed without permission.

Supplementary Materials for

Mechanisms of neutralizing antibody response probed using synthetic virus-like structures

Wei-Yun Wholey[1†], Alexander R. Meyer[1†], Sekou-Tidiane Yoda[1], Bryce Chackerian[2], Julie Zikherman[3], Wei Cheng[1,4*]

[1]*Department of Pharmaceutical Sciences, 428 Church Street, University of Michigan, Ann Arbor, Michigan 48109, USA*

[2]*Department of Molecular Genetics and Microbiology, School of Medicine, University of New Mexico, Albuquerque, New Mexico 87131, USA*

[3]*Division of Rheumatology, Rosalind Russell and Ephraim P. Engleman Arthritis Research Center, Department of Medicine, University of California, San Francisco, California 94143 USA*

[4]*Department of Biological Chemistry, 1150 W. Medical Center Dr., University of Michigan Medical School, Ann Arbor, Michigan 48109, USA*

Correspondence to: chengwe@umich.edu

These supplementary materials include:

Figs. S1 to S9

Tables S1 to S5

bioRxiv preprint doi: https://doi.org/10.1101/2023.02.20.529089; this version posted February 21, 2023. The copyright holder for this preprint (which was not certified by peer review) is the author/funder. All rights reserved. No reuse allowed without permission.

Fig. S1. Characterization of RBD-conjugated SVLS using a single-molecule fluorescence approach.

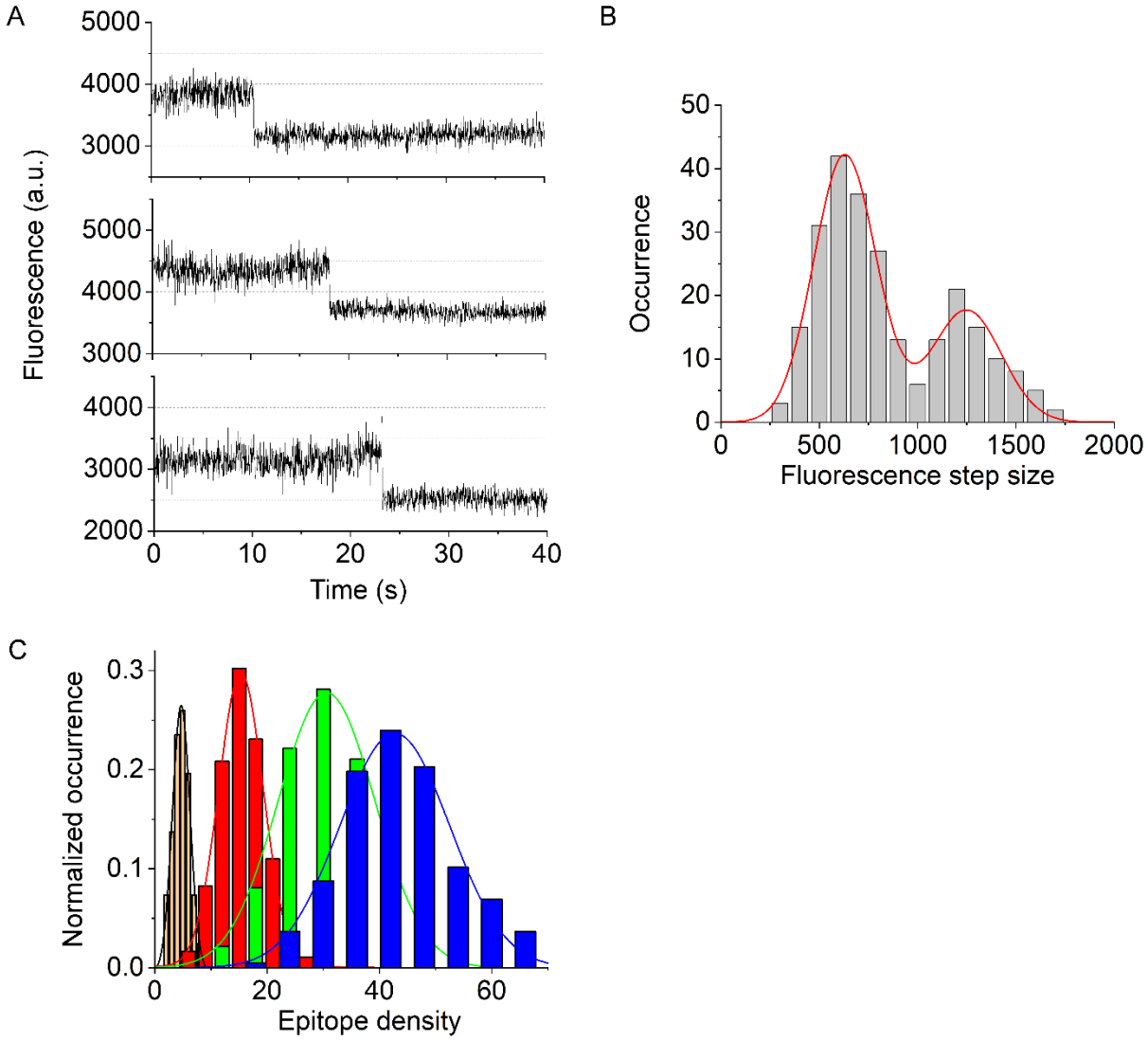

(**A**) Representative single-molecule fluorescence trajectories from Alexa-594 labeled RBD-specific Fab (Alexa-594-Fab). We prepared Alexa-594-Fab using a monoclonal IgG2a specific for SARS-CoV-2 RBD (Biolegend #944803, mAb1 herein). This high-affinity Fab allowed us to quantitate epitope density on individual SVLS conjugated with RBD, using single-molecule fluorescence techniques that we established previously (*33-35*). Briefly, the Fab was prepared from the IgG form of the antibody using a Pierce^{TM} Fab Micro preparation kit (ThermoFisher Scientific, CAT#44685) following manufacturer instructions. The purified Fab was then labeled using Alexa Fluor 594 succinimidyl NHS ester (ThermoFisher Scientific, CAT#A37572) following the protocol that we established previously (*34*). The labeling ratio between the dye and protein was determined to be 3.3 dye molecules per Fab based on single-molecule two-photon fluorescence measurement as we described previously (*34*). As shown in Fig. 1E in the main text, we deposited pRBD(DNA1)4 bound with Alexa-594-Fab on poly-L-lysine coated coverslips, and used epi-fluorescence imaging to directly visualize individual SVLS through excitation of the Alexa-594 fluorophore by a 592-nm laser. Individual SVLS showed up as bright spots in a dark background. Neither SVLS alone

bioRxiv preprint doi: https://doi.org/10.1101/2023.02.20.529089; this version posted February 21, 2023. The copyright holder for this preprint (which was not certified by peer review) is the author/funder. All rights reserved. No reuse allowed without permission.

nor free Alexa-594-Fab alone at the same concentrations yielded these bright spots under the microscope. Moreover, no fluorescent spots were visible when Alexa-594-Fab was incubated with control SVLS without RBD conjugation, confirming that these fluorescent spots were specific for SVLS conjugated with RBD but not protein aggregates. In order to determine the number of RBD molecules per SVLS, we chose to work at a laser power of 100 mW. This illumination condition allowed us to collect the initial fluorescence intensity from individual spots, and the constant illumination of the sample under this condition also allowed us to observe the photobleaching of individual fluorophores with time. As shown in Fig. S1A, these photobleaching events display a hallmark feature of 'steps', where the fluorescence persists for a finite time followed by a sudden decrease in fluorescence intensity. These steps correspond to the photobleaching of individual molecules. We have used a step-detection algorithm that we developed previously (*71*) to identify steps from these real-time fluorescence traces. Measurement of this 'step' size yields the fluorescence intensity of a single Alexa-594 fluorophore, which can be used as an internal reference to convert the initial fluorescence intensity of individual liposomes to the number of Alexa-594 fluorophores, as we have done previously for individual HIV-1 virions (*35*) and individual protein-conjugated liposomes (*33*) using the same quantitation methodology. (**B**) The histogram of the individual photobleaching step sizes for Alexa-594 molecules (N=247), which could be well described by the sum of two Gaussians (red curve), one centered at 630 ± 15 analog-to-digital units (a.u., mean ± standard error) and the other centered at 1249 ± 40 a.u. Under a statistical significance level of 5%, Pearson's Chi-square test (*72*) selected the double-Gaussian distribution (P-value=0.88) and rejected the single-Gaussian distribution (P-value=0.02) as the model to describe the data. The difference in peak values is close to twofold. As we have observed previously, the secondary peak may result from the photobleaching of two Alexa-594 molecules that occurred almost simultaneously, which could not be resolved by either the finite camera exposure time or the step-finding algorithm (*73, 74*). The fluorescence intensity of a single Alexa-594 fluorophore can then be used to calculate the total number of Alexa-594 molecules per SVLS based on a ratio comparison (*75, 76*) with the initial fluorescence intensity of Alexa-594 associated with individual SVLS. The number of RBD molecules per SVLS was then calculated as the total number of Alexa-594 molecules per SVLS normalized by the average number of Alexa-594 molecules per Fab. (**C**) The distributions of epitope density (ED) for pRBD(DNA1)1 (orange), pRBD(DNA1)2 (red), pRBD(DNA1)3 (green), and pRBD(DNA1)4 (blue). These distributions can be well described with Gaussian probability density function, with means and standard deviations of 5 ± 2 for pRBD(DNA1)1 (N=204), 15 ± 4 for pRBD(DNA1)2 (N=182), 31 ± 9 for pRBD(DNA1)3 (N=185), and 43 ± 10 for pRBD(DNA1)4 (N=217), respectively. These values are very close to the value of ED estimated using the ensemble approach as we established previously (Fig. 1F) (*14-16, 33*).

bioRxiv preprint doi: https://doi.org/10.1101/2023.02.20.529089; this version posted February 21, 2023. The copyright holder for this preprint (which was not certified by peer review) is the author/funder. All rights reserved. No reuse allowed without permission.

Fig. S2. Low or undetectable Ag-specific IgM or IgG2c in mice of B6 genetic background upon a single subcutaneous injection of SVLS without iNA.

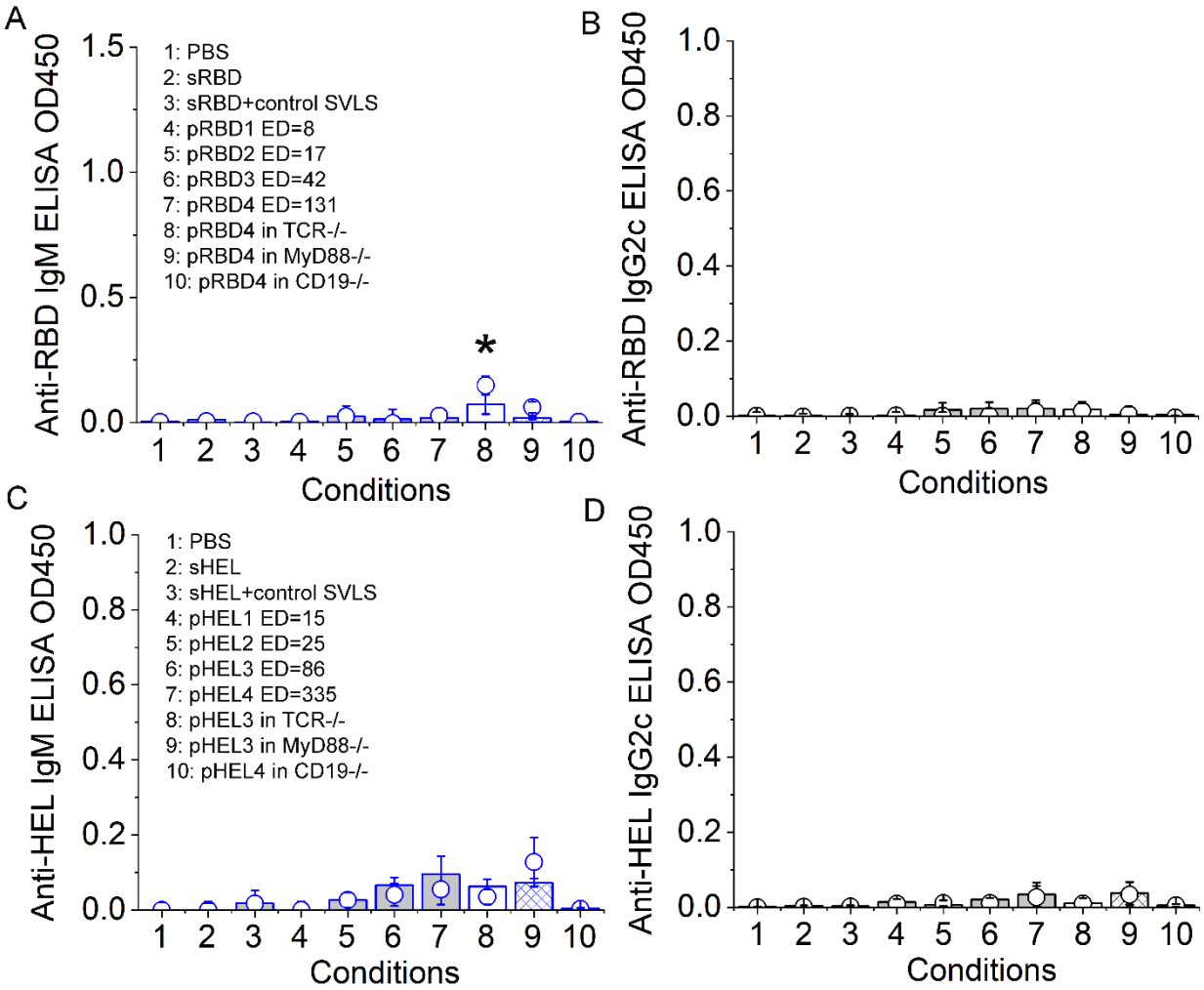

(**A**)(**B**) ELISA OD values for RBD-specific IgM (A) and IgG2c (B) antibody from 1:100 diluted mouse sera after a single subcutaneous injection using various agents listed in the inset with no additional adjuvant. The dose of RBD was 0.24 µg per animal for Conditions 2 through 10. ED refers to epitope density. (**C**)(**D**) ELISA OD values for HEL-specific IgM (C) and IgG2c (D) antibody from 1:100 diluted mouse sera after a single inoculation using various agents listed in the inset. The dose of HEL was 0.3 µg per animal for Conditions 2 through 10. Sera from Day 5 are shown in circles and those from Day 11 post immunization are shown in columns. Graphs depict N=4 mice and are representative of two independent experiments. Throughout Fig. S2, Conditions 1 through 7 were for wtB6 mice. Conditions 8 through 10 were for gene knockout mice of B6 genetic background, with Condition 8 as $TCR^{-/-}$, Condition 9 as $MyD88^{-/-}$ and Condition 10 as $CD19^{-/-}$, following the descriptions in the main text. The pairwise statistical difference between Condition 1 and others on Day 5 was determined by Student's T-test and only Condition 8 in (A) (indicated by the *) shows statistical significance, with p-value < 0.05. Error bars represent the standard errors (N=4).

Fig. S3. Ag-specific IgM and IgG subclasses in BALB/c mice upon a single subcutaneous injection of SVLS without iNA.

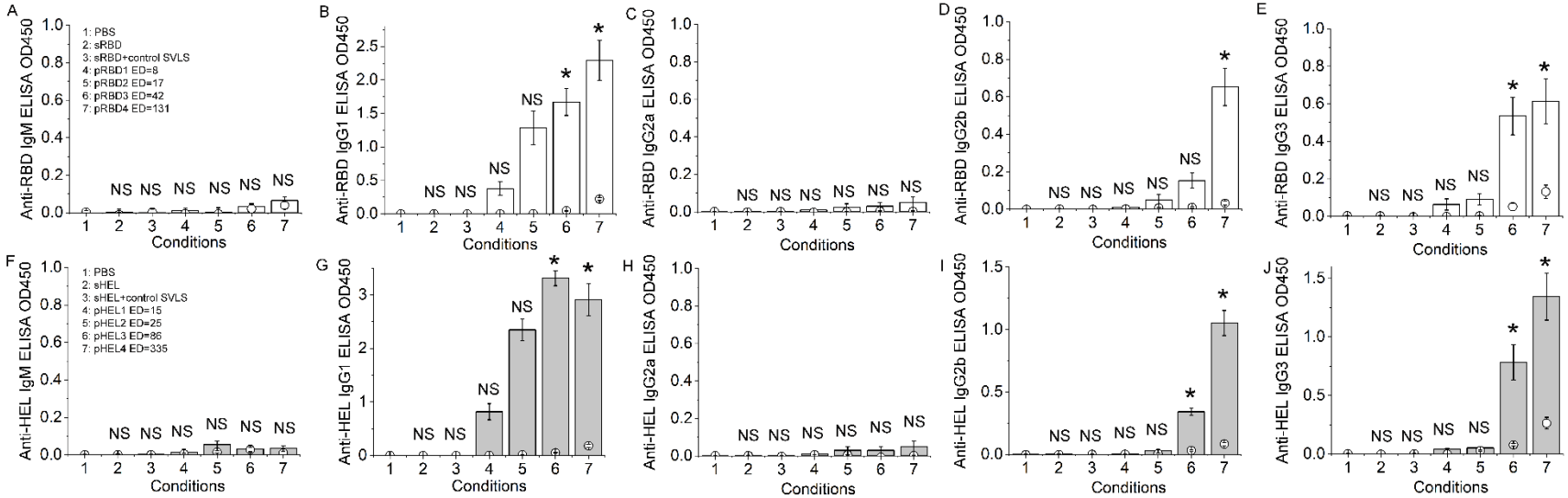

(**A**) through (**E**) ELISA OD values for RBD-specific IgM (A), IgG1 (B), IgG2a (C), IgG2b (D) and IgG3 (E) antibody from 1:100 diluted mouse sera after a single subcutaneous injection using various agents listed in (A) inset with no additional adjuvant. The dose of RBD per injection was 0.24 µg for conditions 2 through 10. (**F**) through (**J**) ELISA OD values for HEL-specific IgM (F), IgG1 (G), IgG2a (H), IgG2b (I) and IgG3 (J) antibody from 1:100 diluted mouse sera after a single subcutaneous injection using various agents listed in (F) inset with no additional adjuvant. The dose of HEL per injection was 0.3 µg for conditions 2 through 10. Throughout, PBS injection (condition 1) was used as a reference to determine the pairwise statistical difference between data points by Student's T-test for all panels. The statistical difference was denoted using the same set of symbols as Fig. 2. Error bars represent the standard errors (N=4).

Fig. S4. Flow cytometry analysis of germinal center B cells from inguinal lymph nodes on Day 12 after injection with various reagents.

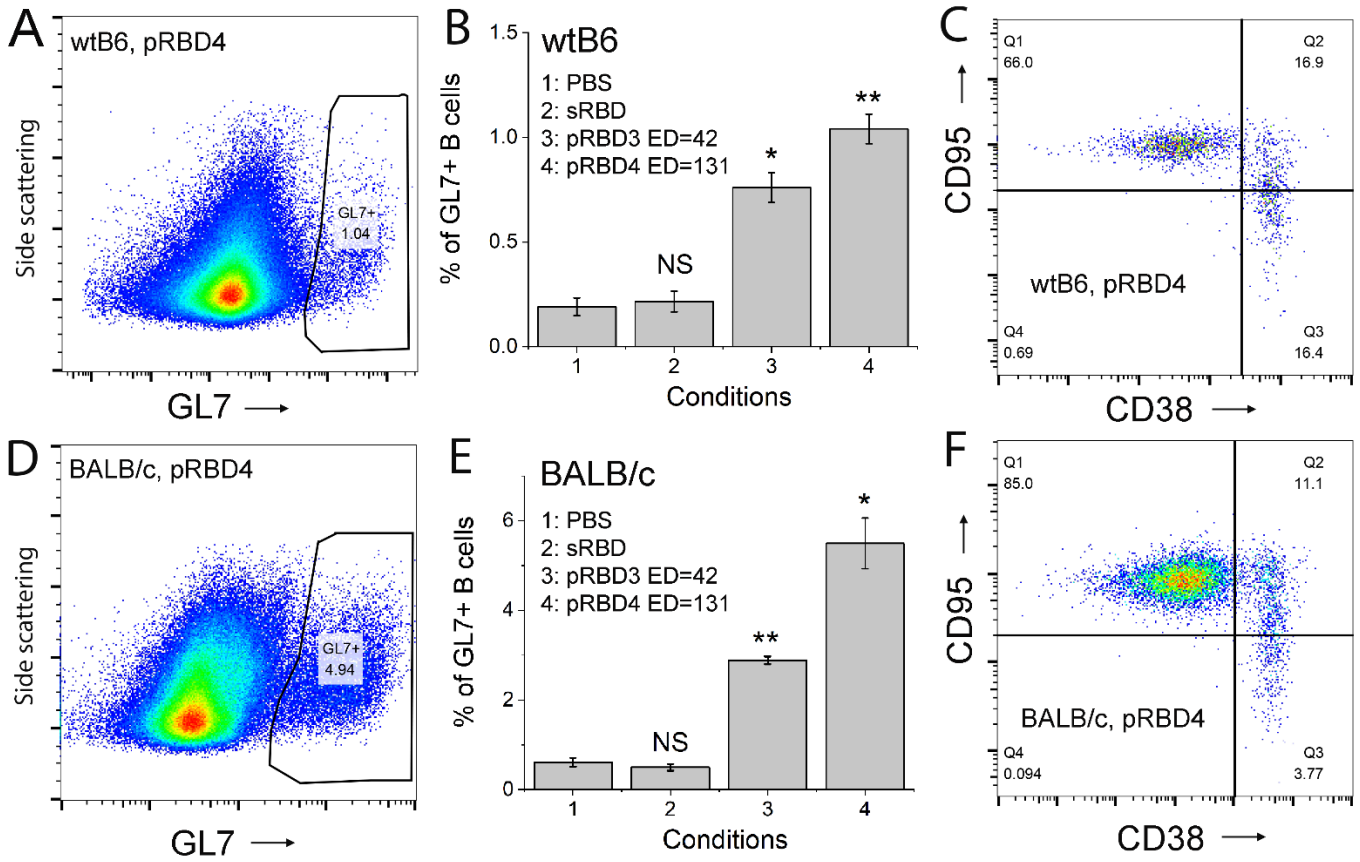

(A) and **(D)**, cytograms showing GL7$^+$ B cells within live CD19$^+$ B cells after a single injection of pRBD4 in wtB6 (A, 198,981 events), and BALB/cJ (D, 164,697 events), respectively. (**B**) and (**E**), percent of GL7$^+$ B cells within live CD19$^+$ B cells after a single injection of various agents in wtB6 (B) and BALB/cJ (E) respectively, including PBS (Condition 1), soluble proteins (Condition 2), pRBD3 (Condition 3), or pRBD4 (Condition 4). PBS-injected mice were used as a reference to determine the pairwise statistical difference between data points by Student's T-test. The statistical difference was denoted using the same set of symbols as Fig. 2. N=4. (**C**) and (**F**), CD38$^-$CD95$^+$ germinal center

B cells, indicated by Q1 in Panel C (1,248 events) and F (6,931 events) and gated by $GL7^+$ $CD19^+$ live B cells from panel A and E, respectively. Throughout Fig. S4, the dose of RBD was 0.48 µg per animal for Conditions 2 through 4.

Fig. S5. Ag-specific IgG subclasses in BALB/c mice upon a single subcutaneous injection of pRBD(DNA1), pHEL(DNA1) or Qβ conjugates.

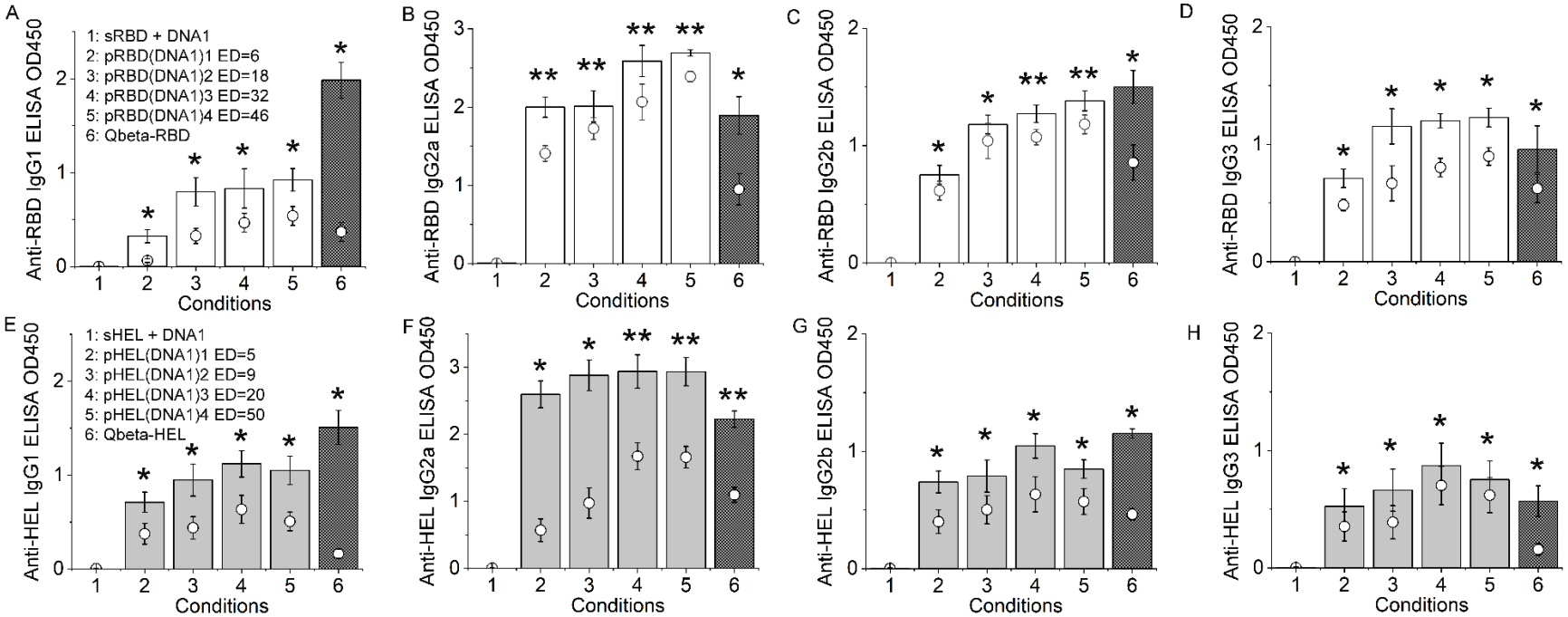

(**A**) through (**D**) ELISA OD values for RBD-specific IgG1 (A), IgG2a (B), IgG2b (C) and IgG3 (D) antibody from 1:100 diluted mouse sera after a single subcutaneous injection using various agents listed in (A) inset with no additional adjuvant. Throughout, the dose of RBD per injection was 0.24 µg for conditions 1 through 6. An admixture of soluble RBD and DNA1 (condition 1) was used as a reference to determine the pairwise statistical difference between data points by Student's T-test. (**E**) through (**H**) ELISA OD values for HEL-specific IgG1 (E), IgG2a (F), IgG2b (G) and IgG3 (H) antibody from 1:100 diluted mouse sera after a single subcutaneous injection using various agents listed in (E) inset with no additional adjuvant. Throughout, the dose of HEL per injection was 0.1 µg for conditions 1 through 6. An admixture of soluble HEL and DNA1 (condition 1) was used as a reference to determine the pairwise statistical difference between data points by Student's T-test. The statistical difference was denoted using the same set of symbols as Fig. 2. Error bars represent the standard errors (N=4). The dose of DNA1 in the admixture with soluble proteins was 1 nmol.

bioRxiv preprint doi: https://doi.org/10.1101/2023.02.20.529089; this version posted February 21, 2023. The copyright holder for this preprint (which was not certified by peer review) is the author/funder. All rights reserved. No reuse allowed without permission.

Fig. S6. Ag-specific IgM in mice of B6 genetic background and BALB/c mice upon a single subcutaneous injection of SVLS with iNA or Qβ-conjugates.

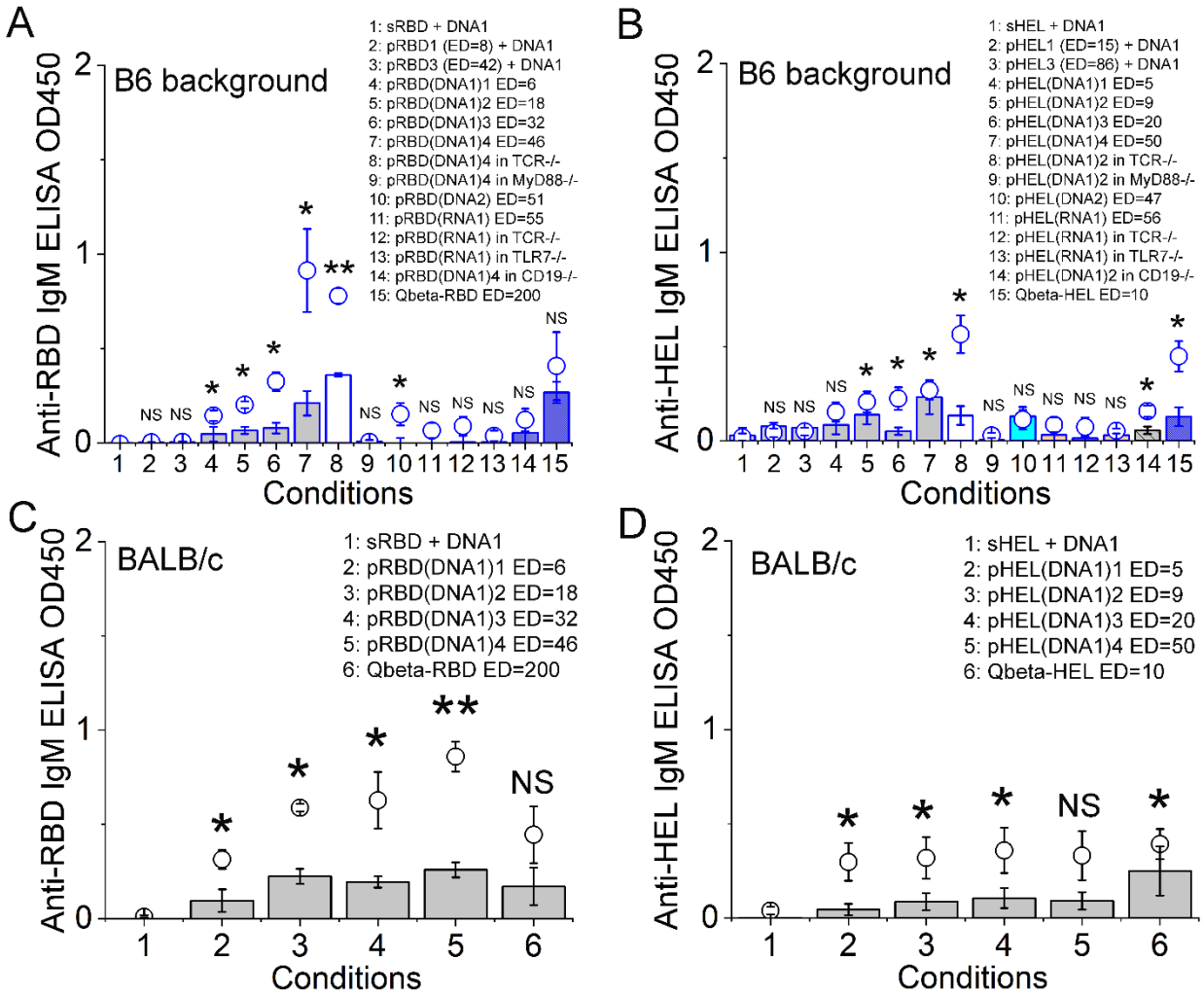

(**A**) ELISA OD values for RBD-specific IgM antibody from 1:100 diluted mouse sera after a single subcutaneous injection using various agents listed in (A) inset with no additional adjuvant in mice of B6 genetic background. The dose of RBD per injection was 0.24 µg for conditions 1 through 15. (**B**) ELISA OD values for HEL-specific IgM antibody from 1:100 diluted mouse sera after a single subcutaneous injection using various agents listed in (B) inset with no additional adjuvant in mice of B6 genetic background. The dose of HEL per injection was 0.1 µg for conditions 1 through 15. (**C**) ELISA OD values for RBD-specific IgM antibody from 1:100 diluted mouse sera after a single subcutaneous injection using various agents listed in (C) inset with no additional adjuvant in BALB/c mice. The dose of RBD per injection was 0.24 µg for conditions 1 through 6. (**D**) ELISA OD values for HEL-specific IgM antibody from 1:100 diluted mouse sera after a single subcutaneous injection using various agents listed in (D) inset with no additional adjuvant in BALB/c mice. The dose of HEL per injection was 0.1 µg for conditions 1 through 6. For each panel above, the respective Condition 1 was used as a reference to determine the pairwise statistical difference between data points within each panel by Student's T-test. Throughout, the statistical difference was denoted using the same set of symbols as Fig. 2. Error bars represent the standard errors (N=4). The dose of DNA1 in admixture with soluble proteins was 1 nmol.

bioRxiv preprint doi: https://doi.org/10.1101/2023.02.20.529089; this version posted February 21, 2023. The copyright holder for this preprint (which was not certified by peer review) is the author/funder. All rights reserved. No reuse allowed without permission.

Fig. S7. Validation of low-density coating of streptavidin sensors in BioLayer interferometry experiments.

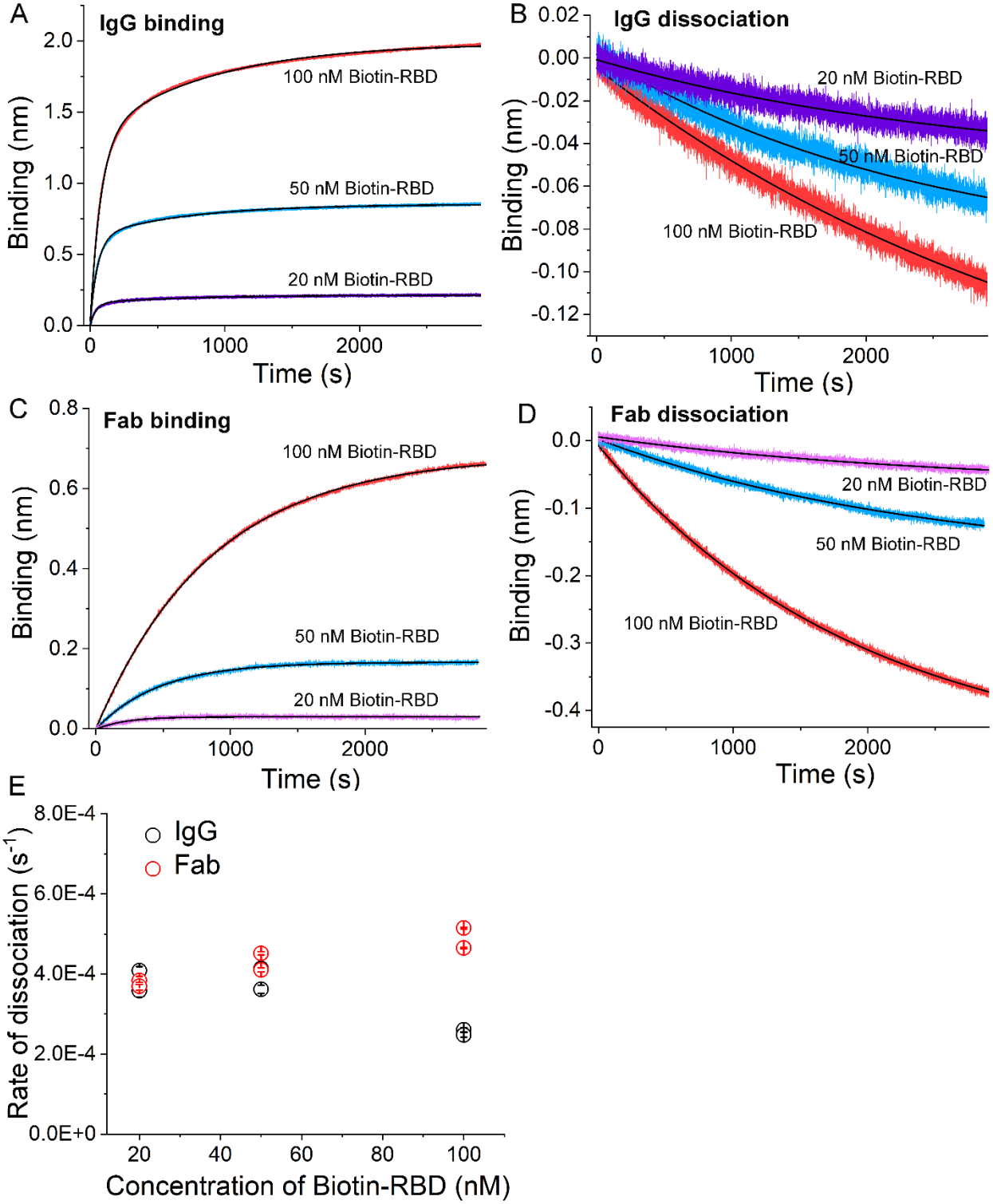

(**A**)(**B**) Real-time binding for mAb1 to biotin-RBD and its dissociation measured using BioLayer interferometry, in which mAb1 is a commercial monoclonal IgG2a specific for SARS-CoV-2 RBD (Biolegend #944803). The streptavidin sensor was coated initially with home-made biotin- RBD at three different concentrations, 20, 50 and 100 nM, as indicated inside each figure panel. The concentration of the IgG was 38 nM. (**C**)(**D**) Real-time binding for a Fab fragment to biotin-RBD and its dissociation measured using BioLayer

bioRxiv preprint doi: https://doi.org/10.1101/2023.02.20.529089; this version posted February 21, 2023. The copyright holder for this preprint (which was not certified by peer review) is the author/funder. All rights reserved. No reuse allowed without permission.

interferometry. The Fab fragment was prepared from mAb1 as described in Fig. S1. The streptavidin sensor was coated initially with home-made biotin-RBD at three different concentrations, 20, 50 and 100 nM, as indicated inside each figure panel. The concentration of the Fab was 62 nM. (A) through (D), the solid black lines were fits to both the binding and dissociation curves using exponential functions. Specifically, all the dissociation curves could be well described with single-exponential function and the exponent returned the rate constant of dissociation. (E) The rate constant of dissociation was plotted as a function of the concentration of biotin-RBD that was used to coat streptavidin sensors. The rate constants for IgG was shown in black circles while the rate constants for the corresponding Fab was shown in red circles. The rate constants from two independent repeats of the same experiments were plotted for both IgG and Fab, respectively. For the rate constants of IgG dissociation from streptavidin sensor of three different coating densities, a one-way ANOVA test returned a p-value of 0.03428, demonstrating that at the 0.05 level, the population means are significantly different. Specifically, the rate of dissociation from the 100-nM biotin-RBD surface was lower than that of either 20 nM or 50 nM biotin-RBD surface. This result is consistent with bivalent binding by IgG on streptavidin sensors coated with 100-nM biotin-RBD, but not for the other two conditions. For the rate constants of Fab dissociation from streptavidin sensor of three different coating densities, a one-way ANOVA test returned a p-value of 0.05601, demonstrating that at the 0.05 level, the population means are not significantly different. Specifically, the rate of dissociation from the 100-nM biotin-RBD surface was statistically indistinguishable from that of either 20 nM or 50 nM biotin-RBD surface. This result is consistent with monovalent binding by Fab on the streptavidin sensor throughout all three coating conditions. Furthermore, a one-way ANOVA test on the following 5 sets of rates of dissociation returned a p-value of 0.06043: IgG dissociation from sensors coated with 20 nM biotin-RBD, IgG dissociation from sensors coated with 50 nM biotin-RBD, Fab dissociation from sensors coated with 20 nM biotin-RBD, Fab dissociation from sensors coated with 50 nM biotin-RBD, and Fab dissociation from sensors coated with 100 nM biotin-RBD. This shows that at the 0.05 level, none of these rate constants are significantly different from one another, and thus demonstrates that IgG binds to sensors coated with either 20 or 50 nM biotin-RBD in a monovalent manner. As a consequence, we have chosen 50 nM biotin-RBD for all BioLayer interferometry experiments.

bioRxiv preprint doi: https://doi.org/10.1101/2023.02.20.529089; this version posted February 21, 2023. The copyright holder for this preprint (which was not certified by peer review) is the author/funder. All rights reserved. No reuse allowed without permission.

Fig. S8. Indicator of affinity maturation that is largely independent of sera IgG concentrations.

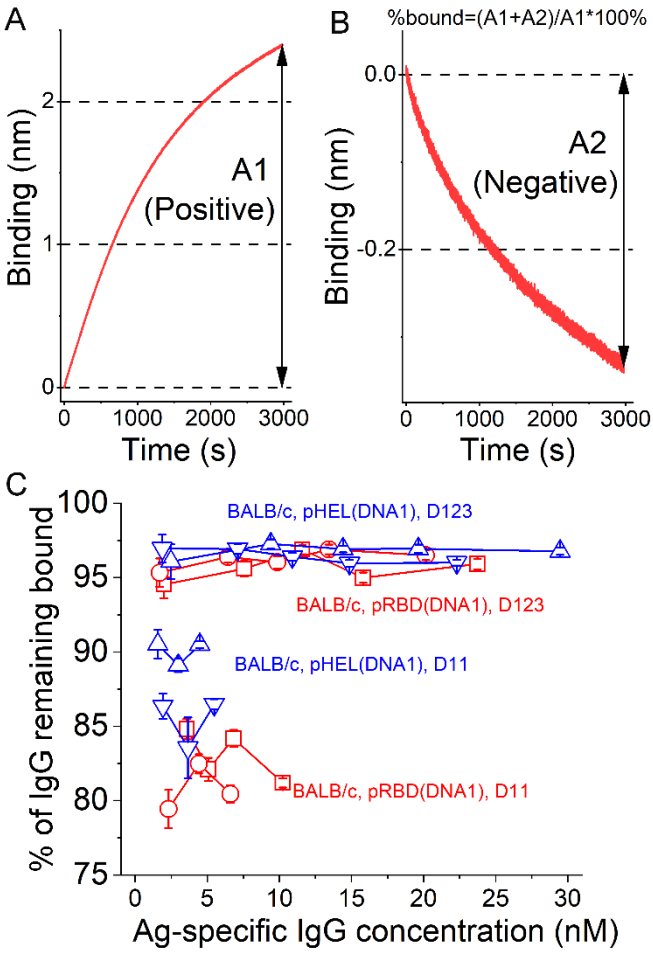

(**A**) A representative of sera IgG binding curve showing the definition of binding amplitude, A1, that is measured from BioLayer interferometry experiments. A1 is the difference in the binding signal between the end and the beginning of a binding curve, which takes a positive value with a unit of nm. (**B**) The corresponding dissociation curve from (A) showing the definition of dissociation amplitude, A2, that is measured from BioLayer interferometry experiments. A2 is the difference in the binding signal between the end and the beginning of a dissociation curve, which takes a negative value with a unit of nm. The percentage of IgG remaining bound at the end of dissociation is calculated as indicated on top of panel (B). (**C**) The percentage of IgG that remains bound at the end of dissociation was plotted as a function of the Ag-specific IgG concentration. For each color and symbol, the different concentrations were realized by dilution of the sera and then BioLayer interferometry experiments were conducted. This was done for several serum samples from BALB/c mice immunized with the agents as noted in the figure. Specifically, red squares, red circles, upper triangles, and down triangles are for pRBD(DNA1)3, pRBD(DNA1)4, pHEL(DNA1)1, and pHEL(DNA1)2, respectively. The dose of RBD was 0.24 µg per animal and the dose of HEL was 0.1 µg per animal. The concentrations for Ag-specific IgG were determined using magnetic beads capture as described in Materials and Methods.

bioRxiv preprint doi: https://doi.org/10.1101/2023.02.20.529089; this version posted February 21, 2023. The copyright holder for this preprint (which was not certified by peer review) is the author/funder. All rights reserved. No reuse allowed without permission.

Fig. S9. A representative standard curve from quantitative western blots to determine the mass of Ag-specific IgG in mouse sera.

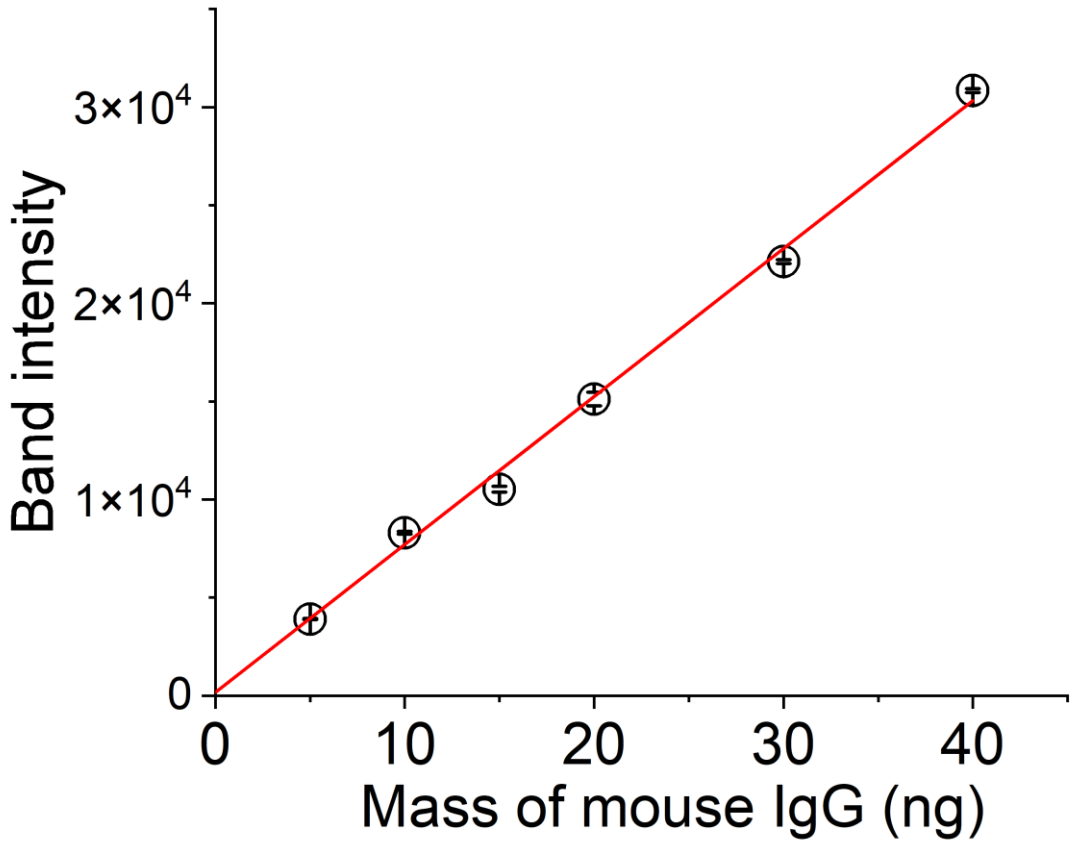

We used mAb1, the commercial monoclonal mouse IgG (Biolegend CAT#944803) as the known reference to construct a standard curve on the same western blot on which Ag-specific IgG antibodies captured by streptavidin magnetic beads were loaded. The band intensity was quantified using ImageJ and plotted against the loaded references. A linear regression was then used to quantitate the mass of Ag-specific IgG in serum samples.

bioRxiv preprint doi: https://doi.org/10.1101/2023.02.20.529089; this version posted February 21, 2023. The copyright holder for this preprint (which was not certified by peer review) is the author/funder. All rights reserved. No reuse allowed without permission.

Table S1. List of SVLS used in current study, together with the respective epitope density (ED), and the average number of internal nucleic acid (iNA) molecules per structure.

S1A:

Name of SVLS	ED*	# of iNA per SVLS
pRBD1	8±2	0
pRBD2	17±2	0
pRBD3	42±3	0
pRBD4	131±9	0
pRBD(DNA1)1	6±1	135±3
pRBD(DNA1)2	18±2	140±4
pRBD(DNA1)3	32±2	152±5
pRBD(DNA1)4	46±2	139±3
pRBD(DNA2)	51±3	138±3
pRBD(RNA1)	55±2	147±4

S1B:

Name of SVLS	ED*	# of iNA per SVLS
pHEL1	15±2	0
pHEL2	25±2	0
pHEL3	86±4	0
pHEL4	335±17	0
pHEL(DNA1)1	5±1	118±3
pHEL(DNA1)2	9±2	128±3
pHEL(DNA1)3	20±2	136±4
pHEL(DNA1)4	50±2	130±3
pHEL(DNA2)	47±2	126±4
pHEL(RNA1)	56±3	135±4

(A) RBD-conjugated SVLS and **(B)** HEL-conjugated SVLS. Throughout, the epitope density (ED) refers to the number of antigenic molecules specifically attached to the SVLS surface through maleimide chemistry. The # of iNA per SVLS refers to the average number of nucleic acid molecules encapsulated inside each SVLS. The uncertainties shown for both ED and iNA are standard errors determined from three independent repeats of the same ensemble experiment. Besides the above SVLS used in this study, control SVLS were SVLS that did not have any protein conjugation on surface nor have any iNA encapsulated inside SVLS.

bioRxiv preprint doi: https://doi.org/10.1101/2023.02.20.529089; this version posted February 21, 2023. The copyright holder for this preprint (which was not certified by peer review) is the author/funder. All rights reserved. No reuse allowed without permission.

Table S2. Statistical comparison of the titer values between SVLS(DNA1) and respective Ag-Qβ conjugates in wtB6 mice.

S2A:

	pRBD(DNA1)1	pRBD(DNA1)2	pRBD(DNA1)3	pRBD(DNA1)4
Qβ-RBD, D5	0.356	0.537	0.024	1.06e-8
Qβ-RBD, D11	2.88e-8	0.024	0.134	N.A.*

Based on the titer values that we measured for pRBD(DNA1) of varied ED and Qβ-RBD (Fig. 3B), we conducted a one-way ANOVA to test the null hypothesis that the means of titers are equal. The resulting p-values from these tests are reported in Table S2A above. At the 0.05 level, the titer for Qβ-RBD on D5 was not statistically different from that of pRBD(DNA1)1 or pRBD(DNA1)2, and was significantly lower than that of pRBD(DNA1)3 or pRBD(DNA1)4. On D11, the titer for Qβ-RBD was statistically higher than that of pRBD(DNA1)1 or pRBD(DNA1)2, and was not statistically different from that of pRBD(DNA1)3 or pRBD(DNA1)4.

*N.A. the titer values for Qβ-RBD and those from pRBD(DNA1)4 were identical within error.

S2B:

	pHEL(DNA1)1	pHEL(DNA1)2	pHEL(DNA1)3	pHEL(DNA1)4
Qβ-HEL, D5	0.207	0.537	1	1
Qβ-HEL, D11	0.134	0.356	0.356	0.356

Based on the titer values that we measured for pHEL(DNA1) of varied ED and Qβ-HEL (Fig. 3D), we conducted a one-way ANOVA to test the null hypothesis that the means of titers are equal. The resulting p-values from these tests are reported in Table S2B above. At the 0.05 level, the titer for Qβ-HEL on D5 was not statistically different from that of pHEL(DNA1)1, pHEL(DNA1)2, pHEL(DNA1)3 or pHEL(DNA1)4. Similarly, on D11, the titer for Qβ-HEL was not statistically different from that of pHEL(DNA1)1, pHEL(DNA1)2, pHEL(DNA1)3 or pHEL(DNA1)4, either.

bioRxiv preprint doi: https://doi.org/10.1101/2023.02.20.529089; this version posted February 21, 2023. The copyright holder for this preprint (which was not certified by peer review) is the author/funder. All rights reserved. No reuse allowed without permission.

Table S3. Statistical comparison of the titer values for SVLS(DNA1) of respective ED between wtB6 and BALB/c mice.

S3A:

	pRBD(DNA1)1	pRBD(DNA1)2	pRBD(DNA1)3	pRBD(DNA1)4
BALB/c, D5	0.356	0.537	0.356	0.134
BALB/c, D11	0.537	0.537	0.134	0.356

Based on the titer values that we measured for pRBD(DNA1) of varied ED in both wtB6 and BALB/c mice (Fig. 3), we conducted a one-way ANOVA to test the null hypothesis that the means of titer values are equal at each respective ED between wtB6 and BALB/c mice. The resulting p-values from these tests are reported in Table S3A above. At the 0.05 level, for each pRBD(DNA1), the titer values from wtB6 mice on D5 or D11 were not statistically different from those in BALB/c mice.

S3B:

	pHEL(DNA1)1	pHEL(DNA1)2	pHEL(DNA1)3	pHEL(DNA1)4
BALB/c, D5	0.537	0.537	0.356	0.356
BALB/c, D11	0.537	0.022	1.408e-8	0.022

Based on the titer values that we measured for pHEL(DNA1) of varied ED in both wtB6 and BALB/c mice (Fig. 3), we conducted a one-way ANOVA to test the null hypothesis that the means of titer values are equal at each respective ED between wtB6 and BALB/c mice. The resulting p-values from these tests are reported in Table S3B above. At the 0.05 level, for each pHEL(DNA1), the titer values from wtB6 mice on D5 were not statistically different from those in BALB/c mice. For pHEL(DNA1)1, the titer values from wtB6 mice on D11 were not statistically different from those in BALB/c mice. However, for pHEL(DNA1)2, pHEL(DNA1)3 and pHEL(DNA1)4, the titer values from BALB/c mice on D11 were statistically higher than those from wtB6 mice.

bioRxiv preprint doi: https://doi.org/10.1101/2023.02.20.529089; this version posted February 21, 2023. The copyright holder for this preprint (which was not certified by peer review) is the author/funder. All rights reserved. No reuse allowed without permission.

Table S4. Statistical comparison of the IgG1 ELISA OD450 values for pRBD(DNA1) of respective ED between wtB6 and BALB/c mice.

	pRBD(DNA1)1	pRBD(DNA1)2	pRBD(DNA1)3	pRBD(DNA1)4
BALB/c, D5	0.512	0.075	0.043	0.609
BALB/c, D11	0.085	0.047	0.444	0.940

Based on the IgG1 ELISA OD450 values that we measured for pRBD(DNA1) of varied ED in both wtB6 and BALB/c mice (Fig. 3G and Fig. S5A), we conducted a one-way ANOVA to test the null hypothesis that the means of ELISA OD450 values are equal at each respective ED between wtB6 and BALB/c mice. The resulting p-values from these tests are reported in Table S4 above. At the 0.05 level, the majority of ELISA OD450 values from wtB6 mice on D5 or D11 were not statistically different from those in BALB/c mice.

bioRxiv preprint doi: https://doi.org/10.1101/2023.02.20.529089; this version posted February 21, 2023. The copyright holder for this preprint (which was not certified by peer review) is the author/funder. All rights reserved. No reuse allowed without permission.

Table S5. A summary of key findings from the current study regarding mechanisms of a nAb response in mice and their implications for understanding viral immunogenicity.

Neutralizing antibody response →

SVLS type	Mouse strains	Initiation (by Day 5)	Amplification (by Day 11)	Duration (Day 12 to 300+)
High ED, no iNA 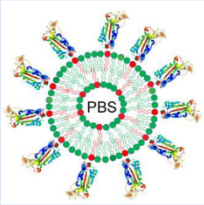	B6	Yes	Yes, but limited compared to BALB/c	Wane with time
		IgG1 IgG2b IgG3 T-cell independent CD19 dependent, MyD88 independent		
	BALB/c	Yes	Yes, with strong IgG1	Grow with time
		IgG1 IgG2b IgG3		
Low ED, with iNA 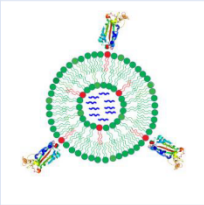	B6	Yes	Yes	Wane with time, but a stronger response than SVLS without iNA
		IgG1 IgG2b IgG2c IgG3 T-cell independent Can be CD19 independent, TLR/MyD88 dependent		
	BALB/c	Yes	Yes	Grow with time, and a stronger response than SVLS without iNA
		IgG1 IgG2a IgG2b IgG3		

Based on current studies, we divide the time dependence of a nAb response into three segments: initiation (by D5), amplification (by D12) and duration (D12 to 300 and beyond). Both SVLS with high ED but without iNA and SVLS with low ED and iNA can induce nAb responses in either B6 or BALB/c mice, although the details in terms of initiation, amplification and duration are different. For SVLS of high ED but without iNA, they initiate a nAb response in B6 mice and the animals produce IgG1, IgG2b and IgG3, like that in BALB/c mice, but the amplification of the nAb response is limited compared to that in BALB/c mice. The nAb level also wanes with time, which contrasts with the nAb response in BALB/c mice that grows with time. BALB/c mice has more IgG1 produced during the stage of amplification. These nAb responses in B6 mice are largely T-cell independent, MyD88 independent but depend on CD19 as revealed by experiments in gene knockout mice of B6 background. For SVLS of low ED with iNA, they initiate nAb responses in both B6 and BALB/c mice and the animals produce IgG1, IgG2c/2a, IgG2b and IgG3. Both the initiation and amplification are similar in these two strains of mice, although the durations are different. The nAb response wanes with time in B6 mice but grows with time in BALB/c mice. For both strains, the nAb responses are much stronger than the responses induced by SVLS without iNA. These nAb responses in B6 mice depend on Toll-like receptors and MyD88 but are largely T-cell independent and can be even mounted in the absence of CD19 as revealed by experiments in gene knockout mice of B6 background. In conclusion, the minimum biochemical constituents required to initiate a nAb response are a foreign protein and lipids. Ag-specific B cells integrate both features of viral signals, i.e., ED and iNA, from individual viral particulate Ags to initiate a nAb response.

bioRxiv preprint doi: https://doi.org/10.1101/2023.02.20.529089; this version posted February 21, 2023. The copyright holder for this preprint (which was not certified by peer review) is the author/funder. All rights reserved. No reuse allowed without permission.

The findings of this study shed light on the immunogenicity of viruses and offer insights that can be applied across different viral infections. The mechanism by which nAbs are produced explains key features of the nAb response in live viral infections, including its speed (*4*), the type of nAb class switch, and the T cell independence of the immediate but potent nAb response (*3, 7-10*) that does not require somatic hypermutation or affinity maturation (*61*).

Lastly, it is important to note that the potency of secreted IgG to neutralize viruses can be affected by ED from the perspective of IgG binding avidity. While low ED on the surface of SVLS with iNA can activate antigen-specific B cells and lead to strong IgG secretion, low ED on the surface of virions can also adversely affect the neutralization potency of the secreted IgG (*36*). This is because a low ED on virion surfaces can impede the bivalent binding of IgG, thereby reducing binding avidity, as has been demonstrated for HIV-1 (*64*).

bioRxiv preprint doi: https://doi.org/10.1101/2023.02.20.529089; this version posted February 21, 2023. The copyright holder for this preprint (which was not certified by peer review) is the author/funder. All rights reserved. No reuse allowed without permission.

REFERENCES

1. M. F. Bachmann, R. M. Zinkernagel, Neutralizing antiviral B cell responses. *Annu Rev Immunol* **15**, 235-270 (1997).
2. J. H. Lam, N. Baumgarth, The Multifaceted B Cell Response to Influenza Virus. *J Immunol* **202**, 351-359 (2019).
3. E. Szomolanyi-Tsuda, R. M. Welsh, T-cell-independent antiviral antibody responses. *Curr Opin Immunol* **10**, 431-435 (1998).
4. L. Hangartner, R. M. Zinkernagel, H. Hengartner, Antiviral antibody responses: the two extremes of a wide spectrum. *Nat Rev Immunol* **6**, 231-243 (2006).
5. M. K. Slifka, R. Ahmed, Long-term humoral immunity against viruses: revisiting the issue of plasma cell longevity. *Trends Microbiol* **4**, 394-400 (1996).
6. E. Szomolanyi-Tsuda, R. M. Welsh, T cell-independent antibody-mediated clearance of polyoma virus in T cell-deficient mice. *J Exp Med* **183**, 403-411 (1996).
7. M. A. Franco, H. B. Greenberg, Immunity to rotavirus in T cell deficient mice. *Virology* **238**, 169-179 (1997).
8. B. O. Lee *et al.*, CD4 T cell-independent antibody response promotes resolution of primary influenza infection and helps to prevent reinfection. *J Immunol* **175**, 5827-5838 (2005).
9. N. Juleff *et al.*, Foot-and-mouth disease virus can induce a specific and rapid CD4+ T-cell-independent neutralizing and isotype class-switched antibody response in naive cattle. *J Virol* **83**, 3626-3636 (2009).
10. L. C. Wang *et al.*, CD4 T-cell-independent antibody response reduces enterovirus 71 lethality in mice by decreasing tissue viral loads. *Clin Dev Immunol* **2012**, 580696 (2012).
11. I. J. Amanna, N. E. Carlson, M. K. Slifka, Duration of humoral immunity to common viral and vaccine antigens. *N Engl J Med* **357**, 1903-1915 (2007).
12. J. M. Dan *et al.*, Immunological memory to SARS-CoV-2 assessed for up to 8 months after infection. *Science* **371**, (2021).
13. B. F. Haynes *et al.*, Strategies for HIV-1 vaccines that induce broadly neutralizing antibodies. *Nat Rev Immunol*, 1-17 (2022).
14. Z. Chen *et al.*, Self-Antigens Displayed on Liposomal Nanoparticles above a Threshold of Epitope Density Elicit Class-Switched Autoreactive Antibodies Independent of T Cell Help. *J Immunol* **204**, 335-347 (2020).
15. W. Y. Wholey *et al.*, Synthetic Liposomal Mimics of Biological Viruses for the Study of Immune Responses to Infection and Vaccination. *Bioconjug Chem* **31**, 685-697 (2020).
16. W. Y. Wholey, S. T. Yoda, W. Cheng, Site-Specific and Stable Conjugation of the SARS-CoV-2 Receptor-Binding Domain to Liposomes in the Absence of Any Other Adjuvants Elicits Potent Neutralizing Antibodies in BALB/c Mice. *Bioconjug Chem* **32**, 2497-2506 (2021).
17. M. F. Bachmann, G. T. Jennings, Vaccine delivery: a matter of size, geometry, kinetics and molecular patterns. *Nat Rev Immunol* **10**, 787-796 (2010).
18. B. Chackerian, D. R. Lowy, J. T. Schiller, Conjugation of a self-antigen to papillomavirus-like particles allows for efficient induction of protective autoantibodies. *J Clin Invest* **108**, 415-423 (2001).
19. I. Yamashita, K. Iwahori, S. Kumagai, Ferritin in the field of nanodevices. *Biochim Biophys Acta* **1800**, 846-857 (2010).
20. N. P. King *et al.*, Computational design of self-assembling protein nanomaterials with atomic level accuracy. *Science* **336**, 1171-1174 (2012).
21. M. Kanekiyo *et al.*, Self-assembling influenza nanoparticle vaccines elicit broadly neutralizing H1N1 antibodies. *Nature* **499**, 102-106 (2013).

bioRxiv preprint doi: https://doi.org/10.1101/2023.02.20.529089; this version posted February 21, 2023. The copyright holder for this preprint (which was not certified by peer review) is the author/funder. All rights reserved. No reuse allowed without permission.

22. J. Marcandalli *et al.*, Induction of Potent Neutralizing Antibody Responses by a Designed Protein Nanoparticle Vaccine for Respiratory Syncytial Virus. *Cell* **176**, 1420-1431 e1417 (2019).
23. A. C. Walls *et al.*, Elicitation of Potent Neutralizing Antibody Responses by Designed Protein Nanoparticle Vaccines for SARS-CoV-2. *Cell* **183**, 1367-1382 e1317 (2020).
24. T. M. Allen, P. R. Cullis, Drug delivery systems: entering the mainstream. *Science* **303**, 1818-1822 (2004).
25. D. J. Irvine, M. A. Swartz, G. L. Szeto, Engineering synthetic vaccines using cues from natural immunity. *Nat Mater* **12**, 978-990 (2013).
26. J. Ingale *et al.*, High-Density Array of Well-Ordered HIV-1 Spikes on Synthetic Liposomal Nanoparticles Efficiently Activate B Cells. *Cell Rep* **15**, 1986-1999 (2016).
27. D. S. Watson, A. N. Endsley, L. Huang, Design considerations for liposomal vaccines: influence of formulation parameters on antibody and cell-mediated immune responses to liposome associated antigens. *Vaccine* **30**, 2256-2272 (2012).
28. N. Pardi, M. J. Hogan, F. W. Porter, D. Weissman, mRNA vaccines - a new era in vaccinology. *Nat Rev Drug Discov* **17**, 261-279 (2018).
29. P. Zhou *et al.*, A pneumonia outbreak associated with a new coronavirus of probable bat origin. *Nature* **579**, 270-273 (2020).
30. A. Harris *et al.*, Influenza virus pleiomorphy characterized by cryoelectron tomography. *Proc Natl Acad Sci U S A* **103**, 19123-19127 (2006).
31. J. A. Briggs, T. Wilk, R. Welker, H. G. Krausslich, S. D. Fuller, Structural organization of authentic, mature HIV-1 virions and cores. *EMBO J* **22**, 1707-1715 (2003).
32. Z. Ke *et al.*, Structures and distributions of SARS-CoV-2 spike proteins on intact virions. *Nature*, (2020).
33. Z. Chen, J. J. Moon, W. Cheng, Quantitation and Stability of Protein Conjugation on Liposomes for Controlled Density of Surface Epitopes. *Bioconjug Chem* **29**, 1251-1260 (2018).
34. Y. Pang, H. Song, J. H. Kim, X. Hou, W. Cheng, Optical trapping of individual human immunodeficiency viruses in culture fluid reveals heterogeneity with single-molecule resolution. *Nat Nanotechnol* **9**, 624-630 (2014).
35. M. C. DeSantis, J. H. Kim, H. Song, P. J. Klasse, W. Cheng, Quantitative Correlation between Infectivity and Gp120 Density on HIV-1 Virions Revealed by Optical Trapping Virometry. *J Biol Chem* **291**, 13088-13097 (2016).
36. J. S. Klein, P. J. Bjorkman, Few and far between: how HIV may be evading antibody avidity. *PLoS Pathog* **6**, e1000908 (2010).
37. W. Cheng, The Density Code for the Development of a Vaccine? *J Pharm Sci* **105**, 3223-3232 (2016).
38. D. M. Knipe, P. M. Howley, *Fields virology*. (Wolters Kluwer/Lippincott Williams & Wilkins Health, Philadelphia, PA, ed. 6th, 2013), pp. 2 volumes.
39. T. Junt *et al.*, Subcapsular sinus macrophages in lymph nodes clear lymph-borne viruses and present them to antiviral B cells. *Nature* **450**, 110-114 (2007).
40. T. Fehr, D. Skrastina, P. Pumpens, R. M. Zinkernagel, T cell-independent type I antibody response against B cell epitopes expressed repetitively on recombinant virus particles. *Proc Natl Acad Sci U S A* **95**, 9477-9481 (1998).
41. A. F. Ochsenbein *et al.*, Correlation of T cell independence of antibody responses with antigen dose reaching secondary lymphoid organs: implications for splenectomized patients and vaccine design. *J Immunol* **164**, 6296-6302 (2000).
42. B. Chackerian, D. R. Lowy, J. T. Schiller, Induction of autoantibodies to mouse CCR5 with recombinant papillomavirus particles. *Proc Natl Acad Sci U S A* **96**, 2373-2378 (1999).
43. Y. Kato *et al.*, Multifaceted Effects of Antigen Valency on B Cell Response Composition and Differentiation In Vivo. *Immunity*, (2020).

bioRxiv preprint doi: https://doi.org/10.1101/2023.02.20.529089; this version posted February 21, 2023. The copyright holder for this preprint (which was not certified by peer review) is the author/funder. All rights reserved. No reuse allowed without permission.

44. J. F. Brooks *et al.*, Molecular basis for potent B cell responses to antigen displayed on particles of viral size. *BioRxiv*, (2023).
45. F. Schmidt *et al.*, Measuring SARS-CoV-2 neutralizing antibody activity using pseudotyped and chimeric viruses. *J Exp Med* **217**, (2020).
46. H. Tesch, F. I. Smith, W. J. Muller-Hermes, K. Rajewsky, Heterogeneous and monoclonal helper T cells induce similar anti-(4-hydroxy-3-nitrophenyl)acetyl (NP) antibody populations in the primary adoptive response. I. Isotype distribution. *Eur J Immunol* **14**, 188-194 (1984).
47. I. S. Grewal, K. D. Moudgil, E. E. Sercarz, Hindrance of binding to class II major histocompatibility complex molecules by a single amino acid residue contiguous to a determinant leads to crypticity of the determinant as well as lack of response to the protein antigen. *Proc Natl Acad Sci U S A* **92**, 1779-1783 (1995).
48. P. Mombaerts *et al.*, Mutations in T-cell antigen receptor genes alpha and beta block thymocyte development at different stages. *Nature* **360**, 225-231 (1992).
49. B. Hou, B. Reizis, A. L. DeFranco, Toll-like receptors activate innate and adaptive immunity by using dendritic cell-intrinsic and -extrinsic mechanisms. *Immunity* **29**, 272-282 (2008).
50. A. L. Gavin *et al.*, Adjuvant-enhanced antibody responses in the absence of toll-like receptor signaling. *Science* **314**, 1936-1938 (2006).
51. R. C. Rickert, J. Roes, K. Rajewsky, B lymphocyte-specific, Cre-mediated mutagenesis in mice. *Nucleic Acids Res* **25**, 1317-1318 (1997).
52. R. C. Rickert, K. Rajewsky, J. Roes, Impairment of T-cell-dependent B-cell responses and B-1 cell development in CD19-deficient mice. *Nature* **376**, 352-355 (1995).
53. R. H. Carter, D. T. Fearon, CD19: lowering the threshold for antigen receptor stimulation of B lymphocytes. *Science* **256**, 105-107 (1992).
54. D. Depoil *et al.*, CD19 is essential for B cell activation by promoting B cell receptor-antigen microcluster formation in response to membrane-bound ligand. *Nat Immunol* **9**, 63-72 (2008).
55. H. Hemmi *et al.*, A Toll-like receptor recognizes bacterial DNA. *Nature* **408**, 740-745 (2000).
56. J. Eckl-Dorna, F. D. Batista, BCR-mediated uptake of antigen linked to TLR9 ligand stimulates B-cell proliferation and antigen-specific plasma cell formation. *Blood* **113**, 3969-3977 (2009).
57. B. Hou *et al.*, Selective utilization of Toll-like receptor and MyD88 signaling in B cells for enhancement of the antiviral germinal center response. *Immunity* **34**, 375-384 (2011).
58. F. Wu *et al.*, A new coronavirus associated with human respiratory disease in China. *Nature* **579**, 265-269 (2020).
59. A. Jegerlehner *et al.*, TLR9 signaling in B cells determines class switch recombination to IgG2a. *J Immunol* **178**, 2415-2420 (2007).
60. J. T. Bates *et al.*, Reversion of somatic mutations of the respiratory syncytial virus-specific human monoclonal antibody Fab19 reveal a direct relationship between association rate and neutralizing potency. *J Immunol* **190**, 3732-3739 (2013).
61. U. Kalinke *et al.*, The role of somatic mutation in the generation of the protective humoral immune response against vesicular stomatitis virus. *Immunity* **5**, 639-652 (1996).
62. R. M. Zinkernagel, Immunology taught by viruses. *Science* **271**, 173-178 (1996).
63. J. Foote, H. N. Eisen, Kinetic and affinity limits on antibodies produced during immune responses. *Proc Natl Acad Sci U S A* **92**, 1254-1256 (1995).
64. R. P. Galimidi *et al.*, Intra-spike crosslinking overcomes antibody evasion by HIV-1. *Cell* **160**, 433-446 (2015).
65. K. K. Van Rompay *et al.*, A vaccine against CCR5 protects a subset of macaques upon intravaginal challenge with simian immunodeficiency virus SIVmac251. *J Virol* **88**, 2011-2024 (2014).
66. J. M. Lund *et al.*, Recognition of single-stranded RNA viruses by Toll-like receptor 7. *Proc Natl Acad Sci U S A* **101**, 5598-5603 (2004).
67. A. Frey, J. Di Canzio, D. Zurakowski, A statistically defined endpoint titer determination method for immunoassays. *J Immunol Methods* **221**, 35-41 (1998).

bioRxiv preprint doi: https://doi.org/10.1101/2023.02.20.529089; this version posted February 21, 2023. The copyright holder for this preprint (which was not certified by peer review) is the author/funder. All rights reserved. No reuse allowed without permission.

68. L. Yurkovetskiy *et al.*, Structural and Functional Analysis of the D614G SARS-CoV-2 Spike Protein Variant. *Cell* **183**, 739-751 e738 (2020).
69. R. I. Connor, B. K. Chen, S. Choe, N. R. Landau, Vpr is required for efficient replication of human immunodeficiency virus type-1 in mononuclear phagocytes. *Virology* **206**, 935-944 (1995).
70. J. H. Kim, H. Song, J. L. Austin, W. Cheng, Optimized Infectivity of the Cell-Free Single-Cycle Human Immunodeficiency Viruses Type 1 (HIV-1) and Its Restriction by Host Cells. *PLoS One* **8**, e67170 (2013).
71. S. G. Arunajadai, W. Cheng, Step detection in single-molecule real time trajectories embedded in correlated noise. *PLoS One* **8**, e59279 (2013).
72. R. D. Evans, Chapter 27. *The Atomic Nucleus (McGraw-Hill)*, Chapter 27 (1969).
73. Y. Pang, H. Song, J. H. Kim, X. Hou, W. Cheng, Optical trapping of individual human immunodeficiency viruses in culture fluid reveals heterogeneity with single-molecule resolution. *Nat Nanotechnol* **9**, 624-630 (2014).
74. X. Hou, W. Cheng, Single-molecule detection using continuous wave excitation of two-photon fluorescence. *Optics letters* **36**, 3185-3187 (2011).
75. V. C. Coffman, J. Q. Wu, Counting protein molecules using quantitative fluorescence microscopy. *Trends Biochem Sci* **37**, 499-506 (2012).
76. J. Lawrimore, K. S. Bloom, E. D. Salmon, Point centromeres contain more than a single centromere-specific Cse4 (CENP-A) nucleosome. *J Cell Biol* **195**, 573-582 (2011).